CHAPTER 17

THE METHOD OF DISCRETE ORDINATES (S_N-APPROXIMATION)

17.1 INTRODUCTION

Like the spherical harmonics method, the *discrete ordinate method* is a tool to transform the equation of transfer (for a gray medium, or on a spectral basis) into a set of simultaneous partial differential equations. Like the P_N-method, the discrete ordinates or S_N-method may be carried out to any arbitrary order and accuracy, although the mathematical formulation of high-order S_N-schemes is considerably less involved. First proposed by Chandrasekhar [1] in his work on stellar and atmospheric radiation, the S_N-method originally received little attention in the heat transfer community. Again like the P_N-method, the discrete ordinates method was first systematically applied to problems in neutron transport theory, notably by Lee [2] and Lathrop [3, 4]. There were some early, unoptimized attempts to apply the method to one-dimensional, planar thermal radiation problems (Love *et al.* [5, 6], Hottel *et al.* [7], Roux and Smith [8, 9]). But only during the past thirty years has the discrete ordinates method been applied to, and optimized for, general radiative heat transfer problems, primarily through the pioneering works of Fiveland [10–13] and Truelove [14–16].

The discrete ordinates method is based on a discrete representation of the directional variation of the radiative intensity. A solution to the transport problem is found by solving the equation of transfer for a set of discrete directions spanning the total solid angle range of 4π. As such, the discrete ordinates method is simply a finite differencing of the directional dependence of the equation of transfer. Integrals over solid angle are approximated by numerical quadrature (e.g., for the evaluation of the radiative source term, the radiative heat flux, etc.).

Today, many numerical heat transfer models use finite volumes rather than finite differences. Similarly, one may also use finite "solid angle volumes" for directional discretization. This variation of the discrete ordinates method is commonly known as the *finite volume method* (for radiative transfer), and enjoys increasing popularity. As a result of the relatively straightforward formulation of high-order implementations, the discrete ordinates method (DOM) and its finite volume cousin (FVM) have received great attention and are today probably the most popular RTE solvers (together with the P_1-approximation), and some version of them is incorporated in most commercial CFD codes. Detailed reviews of the capabilities and shortcomings of the

DOM and FVM have been given by Charest *et al.* [17] and by Coelho [18]. The latter provides the most complete description of the method for general geometries, far exceeding the details we can provide in this book.

In this chapter we shall first develop the set of partial differential equations for the standard S_N-method and their boundary conditions. This is followed by a section describing how the method may be applied to one-dimensional plane-parallel media, and another dealing with spherical and cylindrical geometries, and then its application to two- and three-dimensional problems will be outlined. This is followed by the development of the finite volume method and, finally, the chapter will close with a brief look at other, related methods.

17.2 GENERAL RELATIONS

The general equation of transfer for an absorbing, emitting, and anisotropically scattering medium is, according to equation (10.21),

$$\frac{dI}{ds} = \hat{\mathbf{s}} \cdot \nabla I(\mathbf{r}, \hat{\mathbf{s}}) = \kappa(\mathbf{r}) I_b(\mathbf{r}) - \beta(\mathbf{r}) I(\mathbf{r}, \hat{\mathbf{s}}) + \frac{\sigma_s(\mathbf{r})}{4\pi} \int_{4\pi} I(\mathbf{r}, \hat{\mathbf{s}}') \, \Phi(\mathbf{r}, \hat{\mathbf{s}}', \hat{\mathbf{s}}) \, d\Omega'. \tag{17.1}$$

Equation (17.1) is valid for a gray medium or, on a spectral basis, for a nongray medium, and is subject to the boundary condition

$$I(\mathbf{r}_w, \hat{\mathbf{s}}) = \epsilon(\mathbf{r}_w) I_b(\mathbf{r}_w) + \frac{\rho(\mathbf{r}_w)}{\pi} \int_{\hat{\mathbf{n}} \cdot \hat{\mathbf{s}}' < 0} I(\mathbf{r}_w, \hat{\mathbf{s}}') \, |\hat{\mathbf{n}} \cdot \hat{\mathbf{s}}'| \, d\Omega', \tag{17.2}$$

where we have limited ourselves to an enclosure with opaque, diffusely emitting and diffusely reflecting walls. The extension of equation (17.2) to more complicated boundary conditions is straightforward.

Discrete Ordinates Equations

In the discrete ordinates method, equation (17.1) is solved for a set of n different directions $\hat{\mathbf{s}}_i$, $i = 1, 2, \ldots, n$, and the integrals over direction are replaced by numerical quadratures, that is,

$$\int_{4\pi} f(\hat{\mathbf{s}}) \, d\Omega \simeq \sum_{i=1}^{n} w_i \, f(\hat{\mathbf{s}}_i), \tag{17.3}$$

where the w_i are the quadrature weights associated with the directions $\hat{\mathbf{s}}_i$. Thus, equation (17.1) is approximated by a set of n equations,

$$\hat{\mathbf{s}}_i \cdot \nabla I(\mathbf{r}, \hat{\mathbf{s}}_i) = \kappa(\mathbf{r}) \, I_b(\mathbf{r}) - \beta(\mathbf{r}) \, I(\mathbf{r}, \hat{\mathbf{s}}_i) + \frac{\sigma_s(\mathbf{r})}{4\pi} \sum_{j=1}^{n} w_j \, I(\mathbf{r}, \hat{\mathbf{s}}_j) \, \Phi(\mathbf{r}, \hat{\mathbf{s}}_j, \hat{\mathbf{s}}_i), \quad i = 1, 2, \ldots, n, \tag{17.4}$$

subject to the boundary conditions

$$I(\mathbf{r}_w, \hat{\mathbf{s}}_i) = \epsilon(\mathbf{r}_w) \, I_b(\mathbf{r}_w) + \frac{\rho(\mathbf{r}_w)}{\pi} \sum_{\hat{\mathbf{n}} \cdot \hat{\mathbf{s}}_j < 0} w_j \, I(\mathbf{r}_w, \hat{\mathbf{s}}_j) \, |\hat{\mathbf{n}} \cdot \hat{\mathbf{s}}_j|, \quad \hat{\mathbf{n}} \cdot \hat{\mathbf{s}}_i > 0. \tag{17.5}$$

Each beam traveling in a direction of $\hat{\mathbf{s}}_i$ intersects the enclosure surface twice: once where the beam emanates from the wall ($\hat{\mathbf{n}} \cdot \hat{\mathbf{s}}_i > 0$), and once where it strikes the wall, to be absorbed or reflected ($\hat{\mathbf{n}} \cdot \hat{\mathbf{s}}_i < 0$). The governing equation is first order, requiring only one boundary condition (for the emanating intensity, $\hat{\mathbf{n}} \cdot \hat{\mathbf{s}}_i > 0$). Equations (17.4) together with their boundary conditions (17.5) constitute a set of n simultaneous, first-order, linear partial differential equations for the

unknown $I_i(\mathbf{r}) = I(\mathbf{r}, \hat{\mathbf{s}}_i)$. The solution for the I_i may be found using any standard technique (analytical or numerical). If scattering is present ($\sigma_s \neq 0$), and/or if the bounding walls are reflecting, the equations are coupled in such a way that generally an iterative procedure is necessary. Even in the absence of scattering and surface reflections, the temperature field may not be known, but must be calculated from the intensity field if radiative equilibrium persists, again making iterations necessary. Only in the absence of scattering and wall reflections, and if the temperature field is given, then the solution to the intensities I_i is straightforward (as is the exact solution).

Once the intensities have been determined the desired direction-integrated quantities are readily calculated. The radiative heat flux, inside the medium or at a surface, may be found from its definition, equation (10.52),

$$\mathbf{q}(\mathbf{r}) = \int_{4\pi} I(\mathbf{r}, \hat{\mathbf{s}})\, \hat{\mathbf{s}}\, d\Omega \simeq \sum_{i=1}^{n} w_i\, I_i(\mathbf{r})\, \hat{\mathbf{s}}_i. \tag{17.6}$$

The incident radiation G [and, through equation (10.59), the divergence of the radiative heat flux] is similarly determined as

$$G(\mathbf{r}) = \int_{4\pi} I(\mathbf{r}, \hat{\mathbf{s}})\, d\Omega \simeq \sum_{i=1}^{n} w_i\, I_i(\mathbf{r}). \tag{17.7}$$

At a surface the heat flux may also be determined from surface energy balances [equations (4.1) and (3.16)] as

$$\begin{aligned} \mathbf{q} \cdot \hat{\mathbf{n}}(\mathbf{r}_w) &= \epsilon(\mathbf{r}_w)\,[\pi I_b(\mathbf{r}_w) - H(\mathbf{r}_w)] \\ &\simeq \epsilon(\mathbf{r}_w)\Big(\pi I_b(\mathbf{r}_w) - \sum_{\hat{\mathbf{n}}\cdot\hat{\mathbf{s}}_i<0} w_i\, I_i(\mathbf{r}_w)\, |\hat{\mathbf{n}} \cdot \hat{\mathbf{s}}_i|\Big). \end{aligned} \tag{17.8}$$

Equations (17.4) and (17.5) can be written in a somewhat more compact form if one limits the analysis to linear-anisotropic scattering, i.e., to a scattering phase function of

$$\Phi(\mathbf{r}, \hat{\mathbf{s}}, \hat{\mathbf{s}}') = 1 + A_1(\mathbf{r})\, \hat{\mathbf{s}}' \cdot \hat{\mathbf{s}}. \tag{17.9}$$

Then, using equations (17.6) and (17.7) and/or equation (14.15) leads to

$$\hat{\mathbf{s}}_i \cdot \nabla I_i + \beta I_i = \kappa I_b + \frac{\sigma_s}{4\pi}(G + A_1\, \mathbf{q} \cdot \hat{\mathbf{s}}_i), \quad i = 1, 2, \ldots, n, \tag{17.10}$$

with boundary condition

$$I_i = \frac{J_w}{\pi} = I_{bw} - \frac{1-\epsilon}{\epsilon\pi}\, \mathbf{q} \cdot \hat{\mathbf{n}}, \quad \hat{\mathbf{n}} \cdot \hat{\mathbf{s}}_i > 0 \tag{17.11}$$

at the enclosure surface. Of course, radiative heat flux and incident radiation are unknowns to be determined from directional intensities from the series in equations (17.6) and (17.7). Equations (17.10) and (17.11) are convenient forms for the iterative solution procedure: For each iteration values of G and $\mathbf{q}$ are estimated, and the n intensities I_i are evaluated. The values for G and $\mathbf{q}$ are then updated, and so on.

Selection of Discrete Ordinate Directions

The choice of quadrature scheme is arbitrary, although restrictions on the directions $\hat{\mathbf{s}}_i$ and quadrature weights w_i may arise from the desire to preserve symmetry and to satisfy certain

conditions. It is customary to choose sets of directions and weights that are completely symmetric (i.e., sets that are invariant after any rotation of 90°), and that satisfy the zeroth, first, and second moments, or

$$\int_{4\pi} d\Omega = 4\pi = \sum_{i=1}^{n} w_i, \tag{17.12a}$$

$$\int_{4\pi} \hat{\mathbf{s}}\, d\Omega = \mathbf{0} = \sum_{i=1}^{n} w_i \hat{\mathbf{s}}_i, \tag{17.12b}$$

$$\int_{4\pi} \hat{\mathbf{s}}\hat{\mathbf{s}}\, d\Omega = \frac{4\pi}{3}\boldsymbol{\delta} = \sum_{i=1}^{n} w_i \hat{\mathbf{s}}_i \hat{\mathbf{s}}_i, \tag{17.12c}$$

where $\boldsymbol{\delta}$ is the unit tensor [cf. equation (16.30)]. Different sets of directions and weights satisfying all these criteria have been tabulated, for example, by Lee [2] and Lathrop and Carlson [19]. Fiveland [12] and Truelove [15] have observed that different sets of ordinates may result in considerably different accuracy. They noted that (*i*) the intensity may have directional discontinuity at a wall, and (*ii*) the important radiative heat fluxes at the walls are evaluated through a first moment of intensity over a half range of 2π [equation (17.8)]. They concluded that the set of ordinates and weights should also satisfy the first moment over a half range, that is,

$$\int_{\hat{\mathbf{n}}\cdot\hat{\mathbf{s}}<0} |\hat{\mathbf{n}}\cdot\hat{\mathbf{s}}|\, d\Omega = \int_{\hat{\mathbf{n}}\cdot\hat{\mathbf{s}}>0} \hat{\mathbf{n}}\cdot\hat{\mathbf{s}}\, d\Omega = \pi = \sum_{\hat{\mathbf{n}}\cdot\hat{\mathbf{s}}_i>0} w_i\, \hat{\mathbf{n}}\cdot\hat{\mathbf{s}}_i. \tag{17.13}$$

While it is impossible to satisfy equation (17.13) for arbitrary orientations of the surface normal, it can be satisfied for the principal orientations, if $\hat{\mathbf{n}} = \hat{\mathbf{i}}$, $\hat{\mathbf{j}}$, or $\hat{\mathbf{k}}$. Sets of ordinates and weights that satisfy (*i*) the symmetry requirement, (*ii*) the moment equations (17.12), and (*iii*) the half-moment equation (17.13) (for the three principal directions of $\hat{\mathbf{n}}$)[1] have been given by Lathrop and Carlson [19]. The first four sets labeled S_2-, S_4-, S_6-, and S_8-approximation are reproduced in Table 17.1. In the table the ξ_i, η_i, and μ_i are the direction cosines of $\hat{\mathbf{s}}_i$, or

$$\hat{\mathbf{s}}_i = (\hat{\mathbf{s}}_i\cdot\hat{\mathbf{i}})\,\hat{\mathbf{i}} + (\hat{\mathbf{s}}_i\cdot\hat{\mathbf{j}})\,\hat{\mathbf{j}} + (\hat{\mathbf{s}}_i\cdot\hat{\mathbf{k}})\,\hat{\mathbf{k}} = \xi_i\hat{\mathbf{i}} + \eta_i\hat{\mathbf{j}} + \mu_i\hat{\mathbf{k}}. \tag{17.14}$$

Only positive direction cosines are given in Table 17.1, covering one eighth of the total range of solid angles 4π. To cover the entire 4π any or all of the values of ξ_i, η_i, and μ_i may be positive or negative. Therefore, each row of ordinates contains eight different directions. For example, for the S_2-approximation the different directions are $\hat{\mathbf{s}}_1 = 0.577350(\hat{\mathbf{i}} + \hat{\mathbf{j}} + \hat{\mathbf{k}})$, $\hat{\mathbf{s}}_2 = 0.577350(\hat{\mathbf{i}} + \hat{\mathbf{j}} - \hat{\mathbf{k}})$, ..., $\hat{\mathbf{s}}_8 = -0.577350(\hat{\mathbf{i}} + \hat{\mathbf{j}} + \hat{\mathbf{k}})$. Since the symmetric S_2-approximation does not satisfy the half-moment condition, a nonsymmetric S_2-approximation is also included in Table 17.1, as proposed by Truelove [15]. This approximation satisfies equation (17.13) for two principal directions and should be applied to one- and two-dimensional problems, from which the nonsymmetric term drops out (as seen in Example 17.1 in the following section). The name "S_N-approximation" indicates that N different direction cosines are used for each principal direction. For example, for the S_4-approximation $\xi_i = \pm 0.295876$ and ± 0.908248 (or η_i or μ_i). Altogether there are always $n = N(N+2)$ different directions to be considered (because of symmetry, many of these may be unnecessary for one- and two-dimensional problems). Several other quadrature schemes can be found in the literature. Carlson [20] proposed a set with equal weights w_i (such as the S_2 and S_4 sets in Table 17.1). Two more quadratures and a good review of the applicability of all discrete ordinate sets have been given by Fiveland [21]. Other publications documenting procedures for the generation of quadrature sets are those of Sánchez and Smith [22] and El-Wakil and Sacadura [23]. A new family of quadrature sets, like the S_n

[1] With the exception of the symmetric S_2-approximation.

TABLE 17.1
Discrete ordinates for the S_N-approximation ($N = 2, 4, 6, 8$), from [19].

Order of Approximation	Ordinates			Weights
	ξ	η	μ	w
S_2 (symmetric)	0.5773503	0.5773503	0.5773503	1.5707963
S_2 (nonsymmetric)	0.5000000	0.7071068	0.5000000	1.5707963
S_4	0.2958759	0.2958759	0.9082483	0.5235987
	0.2958759	0.9082483	0.2958759	0.5235987
	0.9082483	0.2958759	0.2958759	0.5235987
S_6	0.1838670	0.1838670	0.9656013	0.1609517
	0.1838670	0.6950514	0.6950514	0.3626469
	0.1838670	0.9656013	0.1838670	0.1609517
	0.6950514	0.1838670	0.6950514	0.3626469
	0.6950514	0.6950514	0.1838670	0.3626469
	0.9656013	0.1838670	0.1838670	0.1609517
S_8	0.1422555	0.1422555	0.9795543	0.1712359
	0.1422555	0.5773503	0.8040087	0.0992284
	0.1422555	0.8040087	0.5773503	0.0992284
	0.1422555	0.9795543	0.1422555	0.1712359
	0.5773503	0.1422555	0.8040087	0.0992284
	0.5773503	0.5773503	0.5773503	0.4617179
	0.5773503	0.8040087	0.1422555	0.0992284
	0.8040087	0.1422555	0.5773503	0.0992284
	0.8040087	0.5773503	0.1422555	0.0992284
	0.9795543	0.1422555	0.1422555	0.1712359

sets symmetric in 90° rotations, but with different arrangement of directions, have been given by Thurgood and coworkers [24], and have been dubbed T_n sets by the authors. These always generate positive weights and are claimed to reduce the so-called "ray effect" (which will be discussed a little later on p. 560). These sets have been further refined by Li and coworkers [25]. A comprehensive review of directional quadrature schemes, including an evaluation of their accuracies, has recently been given by Koch and Becker [26]. None of the above ordinate sets can treat collimated (i.e., unidirectional) irradiation accurately. To address this problem Li and coworkers [27] developed the ISW scheme adding a single ordinate of "infinitely small weight" to the regular quadrature set.

17.3 THE ONE-DIMENSIONAL SLAB

We will first demonstrate how the S_N discrete ordinates method is applied to the simple case of a one-dimensional plane-parallel slab bounded by two diffusely emitting and reflecting isothermal plates. As in previous chapters we shall limit ourselves to linear-anisotropic scattering, although extension to arbitrarily anisotropic scattering is straightforward. We avoid it here to make the steps in the development a little easier to follow. If we choose z as the spatial coordinate between the two plates ($0 \le z \le L$), and introduce the optical coordinate τ with $d\tau = \beta\, dz$ ($0 \le \tau \le \tau_L$), equation (17.4) is transformed to

$$\mu_i \frac{dI_i}{d\tau} = (1-\omega)\, I_b - I_i + \frac{\omega}{4\pi} \sum_{j=1}^{n} w_j\, I_j \left[1 + A_1(\mu_i\mu_j + \xi_i\xi_j + \eta_i\eta_j)\right], \quad i = 1, 2, \ldots, n. \tag{17.15}$$

TABLE 17.2
Discrete ordinates for the one-dimensional S_N-approximation (N = 2, 4, 6, 8).

Order of Approximation	Ordinates μ	Weights w'
S_2 (symmetric)	0.5773503	6.2831853
S_2 (nonsymmetric)	0.5000000	6.2831853
S_4	0.2958759	4.1887902
	0.9082483	2.0943951
S_6	0.1838670	2.7382012
	0.6950514	2.9011752
	0.9656013	0.6438068
S_8	0.1422555	2.1637144
	0.5773503	2.6406988
	0.8040087	0.7938272
	0.9795543	0.6849436

For a one-dimensional slab intensity is independent of azimuthal angle. Since for every ordinate j (with a given μ_j) with a positive value for ξ_j there is another with the same, but negative, value, and since the intensity is the same for both ordinates, the terms involving ξ_j in equation (17.15) add to zero. The same is true for the terms involving η_j, but not for those with μ_j (since the intensity does depend on polar angle θ, and $\mu = \cos\theta$). However, the terms involving μ_j are repeated several times: Each value of μ (counting positive and negative μ-values separately) shown in one row of Table 17.1 corresponds to four different ordinates (combinations of positive and negative values for ξ and η). In addition, a particular value of μ may occur on more than one line of Table 17.1. If all the quadrature weights corresponding to a single μ-value are added together, equation (17.15) reduces to

$$\mu_i \frac{dI_i}{d\tau} = (1-\omega)\, I_b - I_i + \frac{\omega}{4\pi} \sum_{j=1}^{N} w'_j I_j (1 + A_1\, \mu_i \mu_j), \quad i = 1, 2, \ldots, N, \tag{17.16}$$

where the w'_j are the summed quadrature weights. For example, for $\mu = 0.2958759$ in the S_4-approximation the summed quadrature weight is $w' = 4 \times (0.5235987 + 0.5235987) = 4\pi/3$, and so forth. The ordinates and quadrature weights for the one-dimensional slab are listed in Table 17.2. Equation (17.16) could have been found less painfully by using equation (17.10) instead of (17.4), leading directly to

$$\mu_i \frac{dI_i}{d\tau} + I_i = (1-\omega)\, I_b + \frac{\omega}{4\pi}(G + A_1\, q\mu_i), \quad i = 1, 2, \ldots, N. \tag{17.17}$$

Before proceeding to the boundary conditions of equation (17.17) we should recognize that, of the N different intensities, half emanate from the wall at $\tau = 0$ (with $\mu_i > 0$), and the other half from the wall at $\tau = \tau_L$ (with $\mu_i < 0$). Following the notation of Chapter 14, we replace the N different I_i by

$$I_1^+,\ I_2^+,\ \ldots, I_{N/2}^+ \quad \text{and} \quad I_1^-,\ I_2^-,\ \ldots, I_{N/2}^-.$$

Then equation (17.17) may be rewritten as

$$\mu_i \frac{dI_i^+}{d\tau} + I_i^+ = (1-\omega)\, I_b + \frac{\omega}{4\pi}(G + A_1\, q\mu_i), \tag{17.18a}$$

$$-\mu_i \frac{dI_i^-}{d\tau} + I_i^- = (1-\omega)\, I_b + \frac{\omega}{4\pi}(G - A_1\, q\mu_i), \tag{17.18b}$$

$$i = 1, 2, \ldots, N/2; \quad \mu_i > 0.$$

With this notation the boundary conditions for equation (17.18) follow from equations (17.5) or (17.11) as

$$\tau = 0: \quad I_i^+ = J_1/\pi = I_{b1} - \frac{1-\epsilon_1}{\epsilon_1\, \pi} q_1, \tag{17.19a}$$

$$\tau = \tau_L: \quad I_i^- = J_2/\pi = I_{b2} + \frac{1-\epsilon_2}{\epsilon_2\, \pi} q_2, \tag{17.19b}$$

$$i = 1, 2, \ldots, N/2, \quad \mu_i > 0.$$

(For the boundary condition at τ_L the sign switches since $\hat{\mathbf{n}}$ points in the direction opposite to z.)

Radiative heat flux q and incident radiation G are related to the directional intensities through equations (17.6) and (17.7), or

$$q = \sum_{i=1}^{N/2} w_i'\, \mu_i (I_i^+ - I_i^-), \tag{17.20a}$$

$$G = \sum_{i=1}^{N/2} w_i' (I_i^+ + I_i^-). \tag{17.20b}$$

At the two surfaces the radiative heat flux is more conveniently evaluated from equation (17.8) as

$$\tau = 0: \quad q_1 = \quad q(0) = \quad \epsilon_1 \Big(E_{b1} - \sum_{i=1}^{N/2} w_i'\, \mu_i\, I_i^- \Big), \tag{17.21a}$$

$$\tau = \tau_L: \quad q_2 = -q(\tau_L) = -\epsilon_2 \Big(E_{b2} - \sum_{i=1}^{N/2} w_i'\, \mu_i\, I_i^+ \Big). \tag{17.21b}$$

Example 17.1. Consider two large, parallel, gray-diffuse and isothermal plates, separated by a distance L. One plate is at temperature T_1 with emittance ϵ_1, the other is at T_2 with ϵ_2. The medium between the two plates is a gray, absorbing/emitting and linear-anisotropically scattering gas ($n = 1$) with constant extinction coefficient β and single scattering albedo ω. Assuming that radiative equilibrium prevails, determine the radiative heat flux between the two plates using the S_2-approximation.

Solution

For radiative equilibrium we have, from equation (10.59), $I_b = G/4\pi$ and $q = \text{const}$; equations (17.18) and (17.19) become

$$\mu_1 \frac{dI_1^+}{d\tau} + I_1^+ = \frac{1}{4\pi}(G + A_1 \omega \mu_1 q),$$

$$-\mu_1 \frac{dI_1^-}{d\tau} + I_1^- = \frac{1}{4\pi}(G - A_1 \omega \mu_1 q),$$

$$\tau = 0: \quad I_1^+ = J_1/\pi, \qquad \tau = \beta L = \tau_L: \quad I_1^- = J_2/\pi.$$

For the S_2-approximation we have only a single ordinate direction μ_1 (pointing toward τ_L for I_1^+, and toward 0 for I_1^-), where $\mu_1 = 0.57735$ for the symmetric S_2-approximation, and $\mu_1 = 0.5$ for the non-symmetric S_2-approximation [which satisfies the half-range moment, equation (17.13)]. For the simple

S_2-approximation the simultaneous equations (only two in this case) may be separated. We do this here by eliminating I_1^+ and I_1^- in favor of G and q. From equation (17.20), with $w_i' = 2\pi$,

$$\begin{aligned} G &= 2\pi(I_1^+ + I_1^-), \\ q &= 2\pi\,\mu_1(I_1^+ - I_1^-). \end{aligned}$$

Therefore, adding and subtracting the two differential equations and multiplying by 2π leads to

$$\begin{aligned} \frac{dq}{d\tau} + G &= G, \quad \text{or} \quad \frac{dq}{d\tau} = 0, \\ \mu_1\frac{dG}{d\tau} + \frac{1}{\mu_1}q &= A_1\omega\mu_1 q, \quad \text{or} \quad \frac{dG}{d\tau} = -\left(\frac{1}{\mu_1^2} - A_1\omega\right)q. \end{aligned}$$

The first equation is simply a restatement of radiative equilibrium, while the second may be integrated (since q = const), or

$$G = C - \left(\frac{1}{\mu_1^2} - A_1\omega\right)q\tau.$$

This relation contains two unknown constants (C and q), which must be determined from the boundary conditions, that is,

$$\begin{aligned} \tau = 0: \quad I_1^+ &= \frac{1}{4\pi}\left(G + \frac{q}{\mu_1}\right) = J_1/\pi, \\ \tau = \tau_L: \quad I_1^- &= \frac{1}{4\pi}\left(G - \frac{q}{\mu_1}\right) = J_2/\pi, \end{aligned}$$

or

$$\begin{aligned} \tau = 0: \quad 4J_1 &= G + \frac{q}{\mu_1} = C + \frac{q}{\mu_1}, \\ \tau = \tau_L: \quad 4J_2 &= G - \frac{q}{\mu_1} = C - \left(\frac{1}{\mu_1^2} - A_1\omega\right)q\,\tau_L - \frac{q}{\mu_1}. \end{aligned}$$

Subtracting, we obtain,

$$\Psi = \frac{q}{J_1 - J_2} = \frac{2\mu_1}{1 + \left(1/\mu_1^2 - A_1\omega\right)\mu_1\tau_L/2},$$

from which the radiosities may be eliminated through equation (14.48). For the symmetric S_2-approximation, $\mu_1 = 0.57735 = 1/\sqrt{3}$, and with isotropic scattering, $A_1 = 0$, this expression becomes

$$\Psi_{\text{symmetric}} = \frac{1}{\sqrt{3}/2 + 3\tau_L/4}.$$

On the other hand, for the nonsymmetric S_2-approximation ($\mu_1 = 0.5$), also with isotropic scattering,

$$\Psi_{\text{nonsymmetric}} = \frac{1}{1 + \tau_L}.$$

The S_2-approximation is the same as the two-flux method discussed in Section 15.3, and the nonsymmetric S_2-method is nothing but the Schuster–Schwarzschild approximation. Results from the two S_2-approximations are compared in Table 17.3 with those from the P_1-approximation and the exact solution. It is seen that the accuracy of the S_2-method is roughly equivalent to that of the P_1-approximation. The nonsymmetric S_2-approximation is superior to the symmetric one, since the symmetric S_2 does not satisfy the half-moment condition, equation (17.13), and causes substantial errors in the optically thin limit.

As a second example for the one-dimensional discrete ordinates method we shall repeat Example 16.4, which was originally designed to demonstrate the use of the P_3-approximation.

Example 17.2. Consider an isothermal medium at temperature T, confined between two large, parallel black plates that are isothermal at the (same) temperature T_w. The medium is gray and absorbs and

TABLE 17.3
Radiative heat flux through a one-dimensional plane-parallel medium at radiative equilibrium; comparison of S_2- and P_1-approximations.

	$\Psi = q/(J_1 - J_2)$			
τ_L	Exact	S_2 (sym)	S_2 (nonsym)	P_1
0.0	1.0000	1.1547	1.0000	1.0000
0.1	0.9157	1.0627	0.9091	0.9302
0.5	0.7040	0.8058	0.6667	0.7273
1.0	0.5532	0.6188	0.5000	0.5714
5.0	0.2077	0.2166	0.1667	0.2105

emits, but does not scatter. Determine an expression for the heat transfer rates within the medium using the S_2 and S_4 discrete ordinates approximations.

Solution
For this particularly simple case equations (17.18) reduce to

$$\mu_i \frac{dI_i^+}{d\tau} + I_i = I_b,$$
$$-\mu_i \frac{dI_i^-}{d\tau} + I_i = I_b.$$

Since $I_b = \text{const}$, these equations may be integrated right away, leading to

$$I_i^+ = I_b + C^+ e^{-\tau/\mu_i},$$
$$I_i^- = I_b + C^- e^{\tau/\mu_i}.$$

The integration constants C^+ and C^- may be found from boundary conditions (17.19) as

$$\tau = 0: \quad I_i^+ = I_{bw} = I_b + C^+, \quad \text{or} \quad C^+ = I_{bw} - I_b;$$
$$\tau = \tau_L: \quad I_i^- = I_{bw} = I_b + C^- e^{\tau_L/\mu_i}, \quad \text{or} \quad C^- = (I_{bw} - I_b) e^{-\tau_L/\mu_i}.$$

Thus,

$$I_i^+ = I_b + (I_{bw} - I_b) e^{-\tau/\mu_i},$$
$$I_i^- = I_b + (I_{bw} - I_b) e^{-(\tau_L - \tau)/\mu_i}.$$

The radiative heat flux follows then from equation (17.20) as

$$q = \sum_{i=1}^{N/2} w_i' \mu_i (I_{bw} - I_b) \left(e^{-\tau/\mu_i} - e^{-(\tau_L - \tau)/\mu_i} \right),$$

or, in nondimensional form,

$$\Psi = \frac{q}{n^2 \sigma (T_w^4 - T^4)} = \frac{1}{\pi} \sum_{i=1}^{N/2} w_i' \mu_i \left(e^{-\tau/\mu_i} - e^{-(\tau_L - \tau)/\mu_i} \right).$$

For the nonsymmetric S_2-approximation we have $w_1' = 2\pi$ and $\mu_1 = 0.5$, or

$$\Psi_{S_2} = e^{-2\tau} - e^{-2(\tau_L - \tau)}.$$

For the S_4-approximation, $w_1' = 4\pi/3$, $w_2' = 2\pi/3$, $\mu_1 = 0.2958759$, $\mu_2 = 0.9082483$, and $\sum w_i' \mu_i = \pi$, so that

$$\Psi_{S_4} = 0.3945012 \left(e^{-\tau/0.2958759} - e^{-(\tau_L - \tau)/0.2958759} \right) + 0.6054088 \left(e^{-\tau/0.9082483} - e^{-(\tau_L - \tau)/0.9082483} \right).$$

The results should be compared with those of Examples 16.2 and 16.4 for the P_1- and P_3-approximations. Note that the S_N-method goes to the correct optically thick limit ($\tau_L \to \infty$) at the wall, i.e., $\Psi \to 1$ [if the half moment of equation (17.13) is satisfied]. The P_N-approximations, on the other hand, overpredict the optically thick limit for this particular example.

It should be emphasized that this last example—dealing with a nonscattering, isothermal medium—is particularly well suited for the discrete ordinates method. One should not expect that, for a general problem, the S_4-method is easier to apply than the P_3-approximation.

A number of researchers have solved more complicated one-dimensional problems by the discrete ordinates method. Fiveland [12] considered the identical case as presented in this section, but allowed for arbitrarily anisotropic scattering. Solving the system of equations by a finite difference method, he noted that higher-order S_N-methods demand a smaller numerical step $\Delta\tau$, in order to obtain a stable solution. Kumar and coworkers [28] not only allowed arbitrarily anisotropic scattering, but also considered boundaries with specular reflectances as well as boundaries with collimated irradiation (as discussed in Chapter 19). To solve the set of simultaneous first-order differential equations they employed a subroutine from the IMSL software library [29], which is available on many computers. Stamnes and colleagues [30, 31] investigated the same problem as Kumar and coworkers but also allowed for variable radiative properties and a general bidirectional reflection function at the surfaces. They decoupled the set of simultaneous equations using methods of linear algebra and found exact analytical solutions in terms of eigenvalues and eigenvectors that, in turn, were determined using the EISPACK software library [32]. Other examples of the use of the one-dimensional discrete ordinates model as a tool to solve more complex problems may be found in [33–42].

17.4 ONE-DIMENSIONAL CONCENTRIC SPHERES AND CYLINDERS

Applying the discrete ordinates method and taking advantage of the symmetries in a one-dimensional problem is considerably more difficult for concentric spheres and cylinders than for a plane-parallel slab. The reason is that the local direction cosines change while traveling along a straight line of sight through such enclosures.

Concentric Spheres

Consider two concentric spheres of radius R_1 and R_2, respectively. The inner sphere surface has an emittance ϵ_1 and is kept isothermal at temperature T_1, while the outer sphere is at temperature T_2 with emittance ϵ_2. If the temperature within the medium is a function of radius only, then the equation of transfer is given by equation (14.69),

$$\mu \frac{\partial I}{\partial r} + \frac{1-\mu^2}{r} \frac{\partial I}{\partial \mu} + \beta I = \beta S, \tag{17.22a}$$

or, alternatively,

$$\frac{\mu}{r^2} \frac{\partial}{\partial r}(r^2 I) + \frac{1}{r} \frac{\partial}{\partial \mu} \left[(1-\mu^2)\, I \right] + \beta I = \beta S, \tag{17.22b}$$

where $\mu = \cos\theta$ is the cosine of the polar angle, measured from the radial direction (see Fig. 14-5). S is the radiative source function,

$$S(r,\mu) = (1-\omega)\, I_b + \frac{\omega}{2} \int_{-1}^{1} I(r,\mu')\, \Phi(\mu,\mu')\, d\mu', \tag{17.23a}$$

or

$$S(r,\mu) = (1-\omega)\, I_b + \frac{\omega}{4\pi} (G + A_1\, q\mu), \tag{17.23b}$$

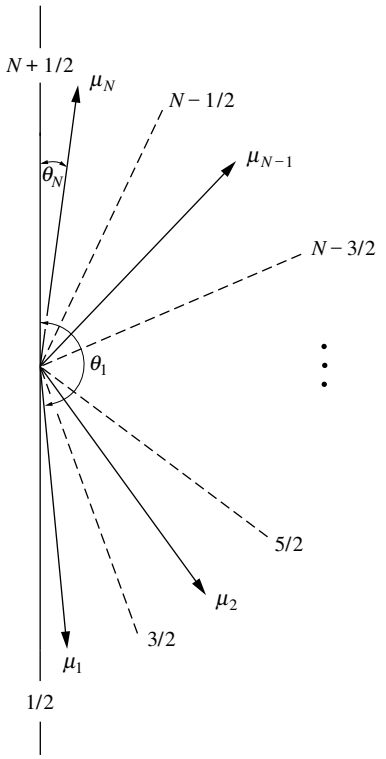

FIGURE 17-1
Directional discretization and discrete ordinate values for one-dimensional problems.

if the scattering is limited to the linear-anisotropic case. The additional difficulty lies in the fact that equation (17.22) contains a derivative over direction cosine, μ, that is to be discretized in the discrete ordinates method. Applying the S_N-method to equation (17.22), we obtain

$$\frac{\mu_i}{r^2}\frac{d}{dr}(r^2 I_i) + \frac{1}{r}\left\{\frac{\partial}{\partial\mu}\left[(1-\mu^2)I\right]\right\}_{\mu=\mu_i} + \beta I_i = \beta S_i, \quad i = 1, 2, \ldots, N, \tag{17.24}$$

where S_i is readily determined from equation (17.23) (and is independent of ordinate direction unless the medium scatters anisotropically). Equation (17.24) is only applied to the N principal ordinates since, similar to the slab, there is no azimuthal dependence. Since the direction vector μ is discretized, its derivative must be approximated by finite differences. We may write

$$\left\{\frac{\partial}{\partial\mu}\left[(1-\mu^2)I\right]\right\}_{\mu=\mu_i} \simeq \frac{\alpha_{i+1/2} I_{i+1/2} - \alpha_{i-1/2} I_{i-1/2}}{w_i'}, \tag{17.25}$$

which is a central difference with the $I_{i\pm1/2}$ evaluated at the boundaries between two ordinates, as shown in Fig. 17-1. Since the differences between any two sequential μ_i are nonuniform, the geometrical coefficients α are nonconstant and need to be determined. The values of α depend only on the differencing scheme and, therefore, are independent of intensity and may be determined by examining a particularly simple intensity field. For example, if both spheres are at the same temperature, then $I_{b1} = I_{b2} = I_b = \text{const}$, and also $I = I_b = \text{const}$. This then leads to

$$\alpha_{i+1/2} - \alpha_{i-1/2} = w_i'\left[\frac{\partial}{\partial\mu}(1-\mu^2)\right]_{\mu=\mu_i} = -2\, w_i'\, \mu_i, \quad i = 1, 2, \ldots, N. \tag{17.26}$$

This expression may be used as a recursion formula for $\alpha_{i+1/2}$, if a value for $\alpha_{1/2}$ can be determined. That value is found by noting that $I_{1/2}$ is evaluated at $\mu = -1$ (Fig. 17-1), where $(1-\mu^2)I = 0$ and,

therefore, $\alpha_{1/2} = 0$. Similarly, $I_{N+1/2}$ is evaluated at $\mu = +1$ and also $\alpha_{N+1/2} = 0$. The finite-difference scheme of equations (17.25) and (17.26) satisfies the relation [4]

$$\begin{aligned}\int_{-1}^{+1} \frac{\partial}{\partial\mu}\left[(1-\mu^2)I\right]d\mu &= (1-\mu^2)\,I\Big|_{-1}^{+1} = 0\\ &= \sum_{i=1}^{N} w_i'\left\{\frac{\partial}{\partial\mu}\left[(1-\mu^2)I\right]\right\}_{\mu=\mu_i} = \sum_{i=1}^{N}\left(\alpha_{i+1/2}I_{i+1/2} - \alpha_{i-1/2}I_{i-1/2}\right)\\ &= \alpha_{3/2}I_{3/2} - \alpha_{1/2}I_{1/2} + \alpha_{5/2}I_{5/2} - \alpha_{3/2}I_{3/2} + - \cdots \alpha_{N+1/2}I_{N+1/2} - \alpha_{N-1/2}I_{N-1/2}\\ &= 0.\end{aligned}$$

Finally, the intensities at the node boundaries, $I_{i\pm1/2}$, need to be expressed in terms of node center values, I_i. We shall use here simple, linear averaging, i.e., $I_{i+1/2} \simeq \frac{1}{2}(I_i + I_{i+1})$. Equation (17.24) may now be rewritten as

$$\frac{\mu_i}{r^2}\frac{d}{dr}(r^2 I_i) + \frac{\alpha_{i+1/2}I_{i+1} + (\alpha_{i+1/2} - \alpha_{i-1/2})I_i - \alpha_{i-1/2}I_{i-1}}{2rw_i'} + \beta I_i = \beta S_i,$$

or, carrying out the differentiation and using equation (17.26),

$$\mu_i\frac{dI_i}{dr} + \frac{\mu_i}{r}I_i + \frac{\alpha_{i+1/2}I_{i+1} - \alpha_{i-1/2}I_{i-1}}{2rw_i'} + \beta I_i = \beta S_i, \tag{17.27a}$$

$$\alpha_{i+1/2} = \alpha_{i-1/2} - 2w_i'\,\mu_i, \quad \alpha_{1/2} = \alpha_{N+1/2} = 0, \quad i = 1, 2, \ldots, N. \tag{17.27b}$$

Equations (17.27) constitute a set of N simultaneous differential equations in the N unknown intensities I_i, subject to the boundary conditions [cf. equation (17.19)]

$$r = R_1 : I_i = J_1/\pi = I_{b1} - \frac{1-\epsilon_1}{\epsilon_1\pi}\,q_1, \quad i = \frac{N}{2}+1, \frac{N}{2}+2, \ldots, N\ (\mu_i > 0), \tag{17.28a}$$

$$r = R_2 : I_i = J_2/\pi = I_{b2} + \frac{1-\epsilon_2}{\epsilon_2\pi}\,q_2, \quad i = 1, 2, \ldots, \frac{N}{2}\ (\mu_i < 0). \tag{17.28b}$$

As for the one-dimensional slab the radiative heat flux and incident radiation are evaluated [cf. equations (17.20) and (17.21)] from

$$G(r) = \sum_{i=1}^{N} w_i'\,I_i(r), \tag{17.29a}$$

$$q(r) = \sum_{i=1}^{N} w_i'\,\mu_i\,I_i(r), \tag{17.29b}$$

and

$$q(R_1) = q_1 = \epsilon_1\Big(E_{b1} + \sum_{\substack{i=1\\(\mu_i<0)}}^{N/2} w_i'\,\mu_i\,I_i\Big), \tag{17.29c}$$

$$-q(R_2) = q_2 = \epsilon_2\Big(E_{b2} - \sum_{\substack{i=N/2+1\\(\mu_i>0)}}^{N} w_i'\,\mu_i\,I_i\Big). \tag{17.29d}$$

Example 17.3. Consider a nonscattering medium at radiative equilibrium that is contained between two isothermal, gray spheres. The absorption coefficient of the medium may be assumed to be gray

and constant. Using the S_2-approximation determine the radiative heat flux between the two concentric spheres.

Solution

From equation (17.27) we find, with $N = 2$, that $\alpha_{1/2} = \alpha_{5/2} = 0$, $\alpha_{3/2} = -2w_1' \mu_1 = 2w_2' \mu_2 = 4\pi\mu$ (since $\mu_2 = -\mu_1 > 0$; we keep $\mu = \mu_2$ as a nonnumerical value to allow comparison between the symmetric and nonsymmetric S_2-approximations). For a gray, nonscattering medium at radiative equilibrium we have $\beta = \kappa$ and $\nabla \cdot \mathbf{q} = 0$, and the source function is, from equations (10.61) and (17.39), $S = I_b = G/4\pi$.

$$
\begin{aligned}
i = 1: \qquad & -\mu \frac{dI_1}{d\tau} - \frac{\mu}{\tau} I_1 + \frac{\mu}{\tau} I_2 + I_1 = \frac{G}{4\pi} = \frac{1}{2}(I_1 + I_2), \\
& -\mu \frac{dI_1}{d\tau} - \left(\frac{\mu}{\tau} - \frac{1}{2}\right)(I_1 - I_2) = 0, \\
i = 2: \qquad & \mu \frac{dI_2}{d\tau} + \frac{\mu}{\tau} I_2 - \frac{\mu}{\tau} I_1 + I_2 = \frac{1}{2}(I_1 + I_2), \\
& \mu \frac{dI_2}{d\tau} - \left(\frac{\mu}{\tau} + \frac{1}{2}\right)(I_1 - I_2) = 0.
\end{aligned}
$$

While addition of the two equations simply leads to a restatement of radiative equilibrium (as in Example 17.1), subtracting them (and multiplying by $w_i' = 2\pi$) leads to

$$
-\mu \frac{d}{d\tau} [2\pi(I_1 + I_2)] + 2\pi(I_1 - I_2) = 0,
$$

or

$$
\frac{dG}{d\tau} = -\frac{q}{\mu^2} = -\frac{\tau^2 q}{\mu^2} \frac{1}{\tau^2}.
$$

Since for a medium at radiative equilibrium between concentric spheres $Q = 4\pi r^2 q = \text{const}$ and, therefore, $\tau^2 q = \text{const}$, the incident radiation may be found by integration,

$$
G(\tau) = \frac{\tau^2 q}{\mu^2} \frac{1}{\tau} + C,
$$

where the two constants ($\tau^2 q$) and C are still unknown and must be determined from the boundary conditions, equations (17.28):

$$
I_2(\tau_1) = J_1/\pi, \quad I_1(\tau_2) = J_2/\pi.
$$

Using the definitions for q and G, equations (17.29),

$$
q = 2\pi\mu (I_2 - I_1) \quad \text{and} \quad G = 2\pi(I_2 + I_1),
$$

or

$$
I_1 = \frac{1}{4\pi}\left(G - \frac{q}{\mu}\right), \; I_2 = \frac{1}{4\pi}\left(G + \frac{q}{\mu}\right),
$$

the boundary conditions may be restated in terms of q and G as

$$
\begin{aligned}
\tau = \tau_1: \qquad & 4J_1 = G + \frac{q_1}{\mu} = \frac{\tau_1 q_1}{\mu^2} + C + \frac{q_1}{\mu} = \frac{\tau^2 q}{\mu^2}\left(\frac{1}{\tau_1} + \frac{\mu}{\tau_1^2}\right) + C, \\
\tau = \tau_2: \qquad & 4J_2 = G - \frac{q_2}{\mu} = \frac{\tau_2 q_2}{\mu^2} + C - \frac{q_2}{\mu} = \frac{\tau^2 q}{\mu^2}\left(\frac{1}{\tau_2} - \frac{\mu}{\tau_2^2}\right) + C.
\end{aligned}
$$

Subtracting the second boundary condition from the first we obtain

$$
\Psi = \frac{\tau^2}{\tau_1^2} \frac{q}{J_1 - J_2} = \frac{1}{\dfrac{1}{4\mu}\left(1 + \dfrac{\tau_1^2}{\tau_2^2}\right) + \dfrac{\tau_1}{4\mu^2}\left(1 - \dfrac{\tau_1}{\tau_2}\right)}.
$$

For the symmetric S_2-approximation, with $\mu = 1/\sqrt{3}$, this equation becomes

$$\Psi_{\text{symmetric}} = \frac{1}{\frac{\sqrt{3}}{4}\left(1 + \frac{\tau_1^2}{\tau_2^2}\right) + \frac{3\tau_1}{4}\left(1 - \frac{\tau_1}{\tau_2}\right)},$$

and for the nonsymmetric approximation with $\mu = 0.5$,

$$\Psi_{\text{nonsymmetric}} = \frac{1}{\frac{1}{2}\left(1 + \frac{\tau_1^2}{\tau_2^2}\right) + \tau_1\left(1 - \frac{\tau_1}{\tau_2}\right)}.$$

The accuracy of the S_2-approximation is very similar to that of the P_1-approximation, for which

$$\Psi_{P_1} = \frac{1}{\frac{1}{2}\left(1 + \frac{\tau_1^2}{\tau_2^2}\right) + \frac{3\tau_1}{4}\left(1 - \frac{\tau_1}{\tau_2}\right)}.$$

Note that the method is very accurate for large τ_1 (large optical thickness) but breaks down for optically thin conditions ($\kappa \to 0$), in particular for small ratios of radii, R_1/R_2. In the limit ($\kappa \to 0$, $R_1/R_2 \to 0$) we find $\Psi_{P_1} = \Psi_{S_2,\text{nonsym}} \to 2$, while the correct limit should go to $\Psi_{\text{exact}} \to 1$.

Numerical solutions to equations (17.27), allowing for anisotropic scattering, variable properties, and external irradiation, have been reported by Tsai and colleagues [43] using the S_8 discrete ordinates method with the equal-weight ordinates of Fiveland [12]. The same method was used by Jones and Bayazitoğlu [44,45] to determine the combined effects of conduction and radiation through a spherical shell.

Concentric Cylinders

The analysis for two concentric cylinders follows along similar lines. Again we consider an absorbing, emitting, and scattering medium contained between two isothermal cylinders with radii R_1 (temperature T_1, diffuse emittance ϵ_1) and R_2 (temperature T_2, emittance ϵ_2), respectively. For this case the equation of transfer is given by equation (14.88),

$$\sin\theta\cos\psi\frac{\partial I}{\partial r} - \frac{\sin\theta\sin\psi}{r}\frac{\partial I}{\partial \psi} + \beta I = \beta S, \tag{17.30}$$

where polar angle θ is measured from the z-axis, and azimuthal angle ψ is measured from the local radial direction (cf. Fig. 14-6). S is the radiative source function and has been given by equation (17.23). Introducing the direction cosines $\xi = \hat{\mathbf{s}} \cdot \hat{\mathbf{e}}_z = \cos\theta$, $\mu = \hat{\mathbf{s}} \cdot \hat{\mathbf{e}}_r = \sin\theta\cos\psi$, and $\eta = \hat{\mathbf{s}} \cdot \hat{\mathbf{e}}_{\psi_c} = \sin\theta\sin\psi$, we may rewrite equation (17.30) as

$$\frac{\mu}{r}\frac{\partial}{\partial r}(rI) - \frac{1}{r}\frac{\partial}{\partial \psi}(\eta I) + \beta I = \beta S. \tag{17.31}$$

For a one-dimensional cylindrical medium the symmetry conditions are not as straightforward as for slabs and spheres. Here we have

$$I(r,\theta,\psi) = I(r,\pi-\theta,\psi) = I(r,\theta,-\psi). \tag{17.32}$$

Therefore, the intensity is the same for positive and negative values of ξ, as well as for positive and negative values of η. Thus, we only need to consider positive values for ξ_i and η_i from Table 17.1, leading to $N_c = N(N+2)/4$ different ordinates for the S_N-approximation, with

quadrature weights $w_i'' = 4w_i$. Equation (17.31) may then be written in discrete ordinates form as

$$\frac{\mu_i}{r}\frac{d}{dr}(rI_i) - \frac{1}{r}\left\{\frac{\partial}{\partial\psi}(\eta I)\right\}_{\psi=\psi_i} + \beta I_i = \beta S_i, \quad i = 1, 2, \ldots, N_c. \tag{17.33}$$

As for the concentric spheres case the term in braces is approximated as

$$\left\{\frac{\partial}{\partial\psi}(\eta I)\right\}_{\psi=\psi_i} \simeq \frac{\alpha_{i+1/2}I_{i+1/2} - \alpha_{i-1/2}I_{i-1/2}}{w_i''}, \quad i = 1, 2, \ldots, N_i,\ \xi_i \text{ fixed}. \tag{17.34}$$

In this relation the subscript $i + 1/2$ implies "toward the next higher value of ψ_i, keeping ξ_i constant." The value of N_i depends on the value of ξ_i. For example, for the S_4-approximation we have from Table 17.1 $N_i = 4$ for $\xi_i = 0.2958759$ (four different values for μ_i, two positive and two negative) and $N_i = 2$ for $\xi_i = 0.9082483$. In the case of concentric cylinders the recursion formula for α, by letting $I = S = \text{const}$ in equation (17.31), is obtained as

$$\alpha_{i+1/2} - \alpha_{i-1/2} = w_i'' \left.\frac{\partial\eta}{\partial\psi}\right|_{\psi=\psi_i} = w_i''\,\mu_i, \quad i = 1, 2, \ldots, N_i,\ \xi_i \text{ fixed}. \tag{17.35}$$

Again, $\alpha_{1/2} = 0$ since at that location $\psi_{1/2} = 0$ and, therefore, $\eta = 0$. Similarly, $\alpha_{N_i+1/2} = 0$ since $\psi_{N_i+1/2} = \pi$ and $\eta = 0$. Finally, using linear averaging for the half-node intensities leads to

$$\mu_i\frac{dI_i}{dr} + \frac{\mu_i}{2r}I_i - \frac{\alpha_{i+1/2}I_{i+1} - \alpha_{i-1/2}I_{i-1}}{2rw_i''} + \beta I_i = \beta S_i, \quad i = 1, 2, \ldots, N_c, \tag{17.36a}$$

$$\alpha_{i+1/2} = \alpha_{i-1/2} + w_i''\,\mu_i, \quad \alpha_{1/2} = \alpha_{N+1/2} = 0, \quad i = 1, 2, \ldots N_i,\ \xi_i \text{ fixed}. \tag{17.36b}$$

Equation (17.36) is the set of equations for concentric cylinders, for the $N_c = N(N+2)/4$ unknown directional intensities I_i, and is equivalent to the set for concentric spheres, equation (17.27). The boundary conditions for cylinders and spheres are basically identical [equations (17.28)], except for some renumbering, as are the expressions for incident intensity and radiative heat flux [equations (17.29)], that is,

$$r = R_1: \quad I_i = \frac{J_1}{\pi} = I_{b1} - \frac{1-\epsilon_1}{\epsilon_1\pi}\,q_1, \quad i = \frac{N_c}{2}+1, \frac{N_c}{2}+2, \ldots, N_c\ (\mu_i > 0), \tag{17.37a}$$

$$r = R_2: \quad I_i = \frac{J_2}{\pi} = I_{b2} + \frac{1-\epsilon_2}{\epsilon_2\pi}\,q_2, \quad i = 1, 2, \ldots, \frac{N_c}{2}\ (\mu_i < 0), \tag{17.37b}$$

$$G(r) = \sum_{i=1}^{N_c} w_i''\,I_i(r), \tag{17.37c}$$

$$q(r) = \sum_{i=1}^{N_c} w_i''\,\mu_i\,I_i(r), \tag{17.37d}$$

and

$$q(R_1) = q_1 = \epsilon_1\Big(E_{b1} + \sum_{\substack{i=1\\(\mu_i<0)}}^{N_c/2} w_i''\,\mu_i\,I_i\Big), \tag{17.37e}$$

$$-q(R_2) = q_2 = \epsilon_2\Big(E_{b2} - \sum_{\substack{i=N_c/2+1\\(\mu_i>0)}}^{N_c} w_i''\,\mu_i\,I_i\Big). \tag{17.37f}$$

An example of the use of the discrete ordinates method in a one-dimensional medium is the work of Krishnaprakas [46], who considered combined conduction and radiation in a gray, constant property medium with various scattering behaviors.

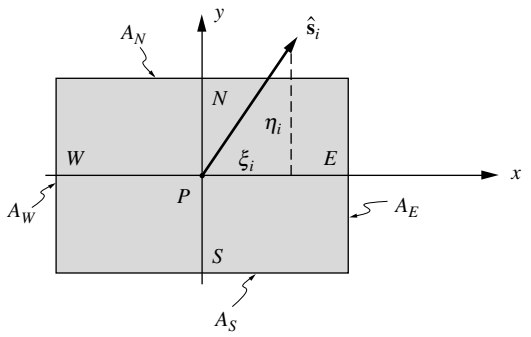

FIGURE 17-2
A general two-dimensional control volume.

17.5 MULTIDIMENSIONAL PROBLEMS

While the discrete ordinates method is readily extended to multidimensional configurations, the method results in a set of simultaneous first-order partial differential equations that generally must be solved numerically. As for one-dimensional geometries, the equation of transfer is slightly different whether a Cartesian, cylindrical, or spherical coordinate system is employed. We shall first describe the method for Cartesian coordinate systems, followed by a brief description of the differences for cylindrical and spherical geometries.

Enclosures Described by Cartesian Coordinates

For Cartesian coordinates equation (17.4) becomes, using equation (17.14),

$$\xi_i \frac{\partial I_i}{\partial x} + \eta_i \frac{\partial I_i}{\partial y} + \mu_i \frac{\partial I_i}{\partial z} + \beta I_i = \beta S_i, \quad i = 1, 2, \ldots, n, \tag{17.38}$$

where S_i is again shorthand for the radiative source function

$$S_i = (1 - \omega) I_b + \frac{\omega}{4\pi} \sum_{j=1}^{n} w_j \Phi_{ij} I_j, \quad i = 1, 2, \ldots, n. \tag{17.39}$$

Equation (17.38) is subject to the boundary conditions in equation (17.5) along each surface. For example, for a surface parallel to the y-z-plane, with $\hat{\mathbf{n}} = \hat{\mathbf{i}}$ and $\hat{\mathbf{n}} \cdot \hat{\mathbf{s}}_j = \hat{\mathbf{s}}_j \cdot \hat{\mathbf{i}} = \xi_j$, we have for all i with $\xi_i > 0$ ($n/2$ boundary conditions)

$$I_i = J_w/\pi = \epsilon_w I_{bw} + \frac{1 - \epsilon_w}{\pi} \sum_{\substack{\xi_j < 0 \\ (n/2 \text{ values})}} w_j I_j |\xi_j|. \tag{17.40}$$

Although the numerical solution to equation (17.38) may be found through standard finite differences, the first order of the equations necessitates backward differencing with large truncation errors. Consequently, it is more common to employ the finite-volume approach of Carlson and Lathrop [4] described below.

Two-Dimensional Problems

For clarity, we shall develop the method here for a two-dimensional geometry (i.e., for $\partial I/\partial z \equiv 0$). For such a problem the intensity is the same for positive and negative values of μ_i. Thus, we need to consider only positive values of μ_i (and double the quadrature weights w_i). A general volume element is shown in Fig. 17-2. The volume element has four face areas A_W and A_E (in the x-direction), and A_S and A_N (in the y-direction). In a simple rectangular enclosure one

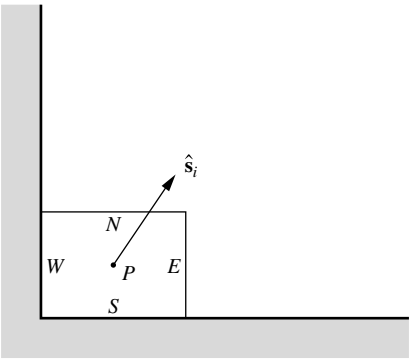

FIGURE 17-3
Enclosure corner, used as starting point for discrete ordinates calculations.

would have (per unit length in the z-direction) $A_W = A_E = \Delta y$, $A_S = A_N = \Delta x$, and $V = \Delta x \Delta y$. The finite-volume formulation of equation (17.38) is obtained by integrating it over a volume element. For example, the term $\partial I_i/\partial x$ transforms to

$$\int_V \frac{\partial I_i}{\partial x}\, dV = \int_{A_E} I_i\, dA_E - \int_{A_W} I_i\, dA_W = I_{Ei}A_E - I_{Wi}A_W, \tag{17.41}$$

where I_{Ei} and I_{Wi} are average values of I_i over the faces of A_E and A_W, respectively. Operating similarly on the other terms changes equation (17.38) to

$$\xi_i(A_E I_{Ei} - A_W I_{Wi}) + \eta_i(A_N I_{Ni} - A_S I_{Si}) = -\beta V I_{pi} + \beta V S_{pi}, \tag{17.42}$$

where I_{pi} and S_{pi} are volume averages. The number of unknowns in equation (17.42) may be reduced by relating cell-edge intensities to the volume-averaged intensity. Most often a linear relationship is chosen, i.e.,

$$I_{pi} = \gamma_y I_{Ni} + (1 - \gamma_y) I_{Si} = \gamma_x I_{Ei} + (1 - \gamma_x) I_{Wi}, \tag{17.43}$$

in which γ_x and γ_y are constants $\frac{1}{2} \le \gamma_x, \gamma_y \le 1$, and the scheme is known as "weighted diamond differencing" as proposed by Carlson and Lathrop [4]. To date most investigators have employed $\gamma_x = \gamma_y = \frac{1}{2}$, simply known as the diamond scheme.

For any point on a surface, boundary conditions are given for all directions pointing *away* from the surface. Therefore, the numerical solution of equation (17.38) customarily proceeds as follows: First, the surface radiosities, J_w, and internal radiative source terms, S_i, are estimated (usually by neglecting reflected surface irradiation and volume in-scattering during the first iteration). Next, the lower left corner (corresponding to minimum values of x and y, as indicated in Fig. 17-3) is chosen as a starting point. From that point all outgoing directions lie in the first quadrant (i.e., both direction cosines ξ_i and η_i are positive). The West and South faces of the control volume in that corner are part of the enclosure surface and, therefore, their intensities I_{Wi} and I_{Si} are known from the boundary conditions. For any discrete ordinate i, the volume-averaged intensity, I_{pi}, of the corner control volume can be calculated by eliminating I_{Ei} and I_{Ni} from equation (17.42) with the help of equation (17.43). Thus,

$$\gamma_x(A_E I_{Ei} - A_W I_{Wi}) = A_E I_{pi} - \left[(1 - \gamma_x)A_E + \gamma_x A_W\right] I_{Wi},$$

etc., and

$$I_{pi} = \frac{\beta V S_{pi} + \xi_i A_{EW} I_{Wi}/\gamma_x + \eta_i A_{NS} I_{Si}/\gamma_y}{\beta V + \xi_i A_E/\gamma_x + \eta_i A_N/\gamma_y}, \tag{17.44}$$

where

$$A_{EW} = (1 - \gamma_x)A_E + \gamma_x A_W, \tag{17.45a}$$

$$A_{NS} = (1 - \gamma_y)A_N + \gamma_y A_S, \tag{17.45b}$$

are averaged face areas. Once I_{pi} has been calculated, I_{Ei} and I_{Ni} are readily determined from equation (17.43), and are equal to the West and South intensities for the adjacent control volumes (for increasing x and y); thus, one by one, the first-quadrant intensities can be calculated for all finite volumes in the enclosure. The procedure is then repeated three times, starting from the remaining three corners of the enclosure, covering the remaining three quadrants of directions. For example, for $\xi_i < 0$, the intensity at the East face of the control volume is known, and the West face intensity must be eliminated from equation (17.42), to be determined after I_{pi} has been found. Thus, we may rewrite equations (17.42) and (17.43) for general (positive or negative) values of ξ_i and η_i as

$$|\xi_i|\,(A_{x_e} I_{x_e i} - A_{x_i} I_{x_i i}) + |\eta_i|\,(A_{y_e} I_{y_e i} - A_{y_i} I_{y_i i}) = -\beta V I_{pi} + \beta V S_i, \tag{17.46}$$

$$I_{pi} = \gamma_x\, I_{x_e i} + (1-\gamma_x)\, I_{x_i i} = \gamma_y\, I_{y_e i} + (1-\gamma_y)\, I_{y_i i}, \tag{17.47}$$

where A_{x_i} is the x-direction face area where the beam enters (= A_W for $\xi_i > 0$, and = A_E for $\xi_i < 0$), A_{x_e} is the x-direction face area through which the beam exits (= A_E for $\xi_i > 0$, and = A_W for $\xi_i < 0$), $I_{y_i i}$ and $I_{y_e i}$ are the corresponding y-direction face intensities, and so on. Then equation (17.44) may be generalized to

$$I_{pi} = \frac{\beta V S_{pi} + |\xi_i|\, A_x I_{x_i i}/\gamma_x + |\eta_i|\, A_y I_{y_i i}/\gamma_y}{\beta V + |\xi_i|\, A_{x_e}/\gamma_x + |\eta_i|\, A_{y_e}/\gamma_y}, \tag{17.48}$$

where

$$A_x = (1-\gamma_x) A_{x_e} + \gamma_x A_{x_i}, \tag{17.49a}$$

$$A_y = (1-\gamma_y) A_{y_e} + \gamma_y A_{y_i}. \tag{17.49b}$$

If all walls are black and in the absence of scattering, all unknown quantities can be calculated with a single pass, since all wall radiosities, J_w, and all internal sources $S_{pi} = (I_b)_{pi}$ are known a priori (if the temperature field is given or assumed). If the walls are reflecting and/or the medium is scattering, iterations are necessary. After a pass over all directions and over all finite volumes has been completed, the values for the wall radiosities and the radiative source terms are updated, and the procedure is repeated until convergence criteria are met. And finally, internal values of incident radiation and radiative heat flux are determined from equations (17.6) and (17.7), while heat fluxes at the walls may be calculated from equations (17.8). For highly reflecting walls ($\epsilon_w \ll 1$) and strongly scattering media ($1 - \omega \ll 1$), the discrete ordinates method will become extremely inefficient. As pointed out by Chai and coworkers [47], the number of iterations caused by scattering can be reduced by removing forward scattering from the phase function, and treating it as transmission. This can be done in equations (17.38) and (17.39) by defining a modified extinction coefficient and a modified source as

$$\beta_{mi} = \beta - \frac{\sigma_s}{4\pi} w_i \Phi_{ii}, \tag{17.50}$$

$$S_{mi} = (1-\omega) I_b + \frac{\omega}{4\pi} \sum_{\substack{j=1 \\ j \neq i}}^{n} w_j \Phi_{ij} I_j, \quad i = 1, 2, ..., n. \tag{17.51}$$

This leads to faster convergence, particularly if the phase function has a strong forward peak (as is often the case for large particles; see also the discussion in Section 12.9).

Spatial Differencing Schemes

Expressing unknown intensities in terms of upstream values, such as defining I_{Ni} and I_{Ei} in terms of I_{pi}, I_{Si}, and I_{Wi} in equation (17.43) for ξ_i, $\eta_i > 0$, is known as spatial differencing (of intensity). Many different schemes have been proposed over the years. We give here only a brief description of the most basic and popular ones.

Step Scheme The step scheme is the simplest differencing scheme, setting $\gamma_x = \gamma_y = 1$, which leads to $I_{Ni} = I_{pi}$ and $I_{Ei} = I_{pi}$ for $\xi_i, \eta_i > 0$, etc. Akin to a fully implicit finite difference of a first derivative, it has the largest truncation error of all methods, but is the only one that never produces unphysical results.

Diamond Scheme This is the most popular differencing scheme, in which the interpolation factors are set to $\gamma_x = \gamma_y = \frac{1}{2}$. However, already Carlson and Lathrop [4] noticed that this may lead to physically impossible negative intensities at the control volume faces (i.e., I_{Ni} and I_{Ei} for $\xi_i, \eta_i > 0$, etc.). While they simply suggest setting negative intensities to zero and continuing computations, this may lead to oscillations and instability. Fiveland [13] showed that such negative intensities may be minimized (but not totally avoided) if finite volume dimensions are kept within

$$\Delta x < \frac{|\xi_i|_{\min}}{\beta(1-\gamma_x)}, \quad \Delta y < \frac{|\eta_i|_{\min}}{\beta(1-\gamma_y)}. \tag{17.52}$$

Therefore, higher-order S_N-approximations (with their smaller minimum value for ξ_i and η_i), as well as optically thick media (large β), require finer volumetric meshes. However, Chai and coworkers [48] have demonstrated that a fine mesh does not guarantee positive intensities, but may in fact *cause* negative intensities. They further noticed that the diamond scheme may result in "overshoot," i.e., predicting unphysically high intensity (intensity leaving a control volume larger than intensity entering plus internal emission).

Exponential Scheme The exponential scheme [4] is generally regarded to be more accurate, particularly for one-dimensional geometries. Here

$$\gamma_s = \frac{1}{1-e^{-\tau_{si}}} - \frac{1}{\tau_{si}}, \quad s = x \text{ or } y; \quad \tau_{xi} = \frac{\beta \Delta x}{\xi_i}, \quad \tau_{yi} = \frac{\beta \Delta y}{\eta_i}. \tag{17.53}$$

Since equation (17.53) leads to interpolation factors less than unity, this method also can lead to physically impossible intensities.

Other relatively simple differencing schemes have been proposed, such as the positive scheme (Lathrop [49]), a variable-weight scheme (Jamaluddin and Smith [50]), an upstream tracing scheme (Chai and colleagues [48]), and a hybrid scheme (Kim and Kim [51]). These methods are somewhat more complex, and have smaller truncation error. However, unlike the simple step scheme they all can lead to unphysical results.

CLAM Scheme The CLAM scheme is a second-order method and, therefore, does not obey equation (17.43). The method is a bounded scheme originally developed for fluid flow problems, and was first applied to radiative heat transfer by Jessee and Fiveland [52]. The intensity *exiting* the control volume at face f (where $f = W, N, E$, or S) is expressed in terms of I_p and center values of adjacent volume elements in the upstream (I_u) and downstream (I_d) directions:

$$I_f = \begin{cases} I_p + \phi(I_d - I_p), & 0 \le \phi \le 1, \\ I_p, & \text{otherwise}, \end{cases} \tag{17.54}$$

where

$$\phi = \frac{I_p - I_u}{I_d - I_u}. \tag{17.55}$$

In the context of Fig. 17-2 for the given direction $\hat{\mathbf{s}}_i$, intensity exits the N face (with d being the volume element above N, and u the volume element below S) and the E face (with d being the volume element to the right of E, and u the one to the left of W). Intensity *entering* the S face exits the N face of the volume element below and equation (17.54) is applied to that element, etc.

Since high-order schemes, such as CLAM, make the set of equations nonlinear, the intensity propagating along a single direction can no longer be evaluated in a single sweep, even in the absence of scattering and/or wall reflection. The equations must be linearized and a solution

is found through iteration, mostly using the "deferred correction" procedure [18]. For the nth iteration equation (17.54) is modified to

$$I_f^n = I_p^n + \phi^{n-1}(I_d^{n-1} - I_p^{n-1}), \tag{17.56}$$

i.e., the first term on the right-hand side is treated implicitly (using the step scheme, $\gamma_x = \gamma_y = 1$), while the remainder is explicit (taking values from the previous iteration, provided $0 \le \phi^{n-1} \le 1$). This way equation (17.48) remains in effect, but includes additional source terms stemming from the explicit terms in equation (17.56).

The CLAM scheme belongs to the class of bounded, high-resolution interpolation schemes based on the Normalized Variable Diagram (NVD) formulation proposed by Leonard [53]. The CLAM scheme is known to be stable and fairly economical and, while other NVD schemes can be more accurate, they also tend to be more time consuming. More detail on spatial differencing schemes may be found in [18, 52, 54]

False Scattering

One of the more serious shortcomings of the discrete ordinates method is *false scattering*, which is a consequence of spatial discretization errors, and is akin to "numerical diffusion" in CFD calculations. If a single, collimated beam is traced through an enclosure by the discrete ordinates method, the beam will gradually widen as it moves farther away from its point of origin. This unphysical smearing of the radiative intensity, even in the absence of real scattering, is known as *false scattering* and can be reduced by using a finer mesh of control volumes.

Ray Effect

Another serious drawback of the method is the so-called "ray effect," which is a consequence of angular discretization. Consider an enclosure with a very small zone (volume or surface area) with very high emission. Intensity from this zone will be carried away from it into the directions of the discrete ordinates. Far away from the emission zone these rays may become so far apart that some control volumes and/or surface zones may not receive any energy from this high-emission zone, leading to unphysical results. Clearly, the ray effect can be reduced by increasing the size of control volumes and surface zones. Therefore, when using a finer spatial mesh to reduce false scattering, this should be accompanied by an increase in the order of the method (i.e., a finer angular quadrature). More discussion on ray effects and how to mitigate them may be found in [55–58].

Example 17.4. A gray, absorbing/emitting (but not scattering) medium is contained within a square enclosure of side lengths L. The medium is at radiative equilibrium and has a constant absorption coefficient such that $\kappa L = 1$. The top and both side walls are at zero temperature, while the bottom wall is isothermal at temperature T_w (with constant blackbody intensity I_{bw}); all four surfaces are black. Calculate the local heat loss from the bottom surface using the discrete ordinates method.

Solution

For the illustrative purposes of this example we shall limit ourselves to the simple nonsymmetric S_2-approximation, with the crude nodal system indicated in Fig. 17-4. For the nonsymmetric S_2-approximation (without dependence in the z-direction) we have to consider four discrete ordinates whose direction vectors (projected into the x-y-plane) are $\hat{\mathbf{s}}_i = \xi_i\hat{\mathbf{i}} + \eta_i\hat{\mathbf{j}} = \pm 0.5(\hat{\mathbf{i}} \pm \hat{\mathbf{j}})$, as given by Table 17.1. The quadrature weight for each direction is, after doubling because of the two-dimensionality, $w_i = \pi$. For radiative equilibrium in a gray, nonscattering medium $\nabla \cdot \mathbf{q} = 0$, and the source function is, from equations (10.61) and (17.39), $S = I_b = G/4\pi$, which is not a function of direction.

We will first solve the problem with the popular diamond spatial differencing scheme, i.e., $\gamma_x = \gamma_y = \frac{1}{2}$. Since all nodal surface areas are $A = L/2$, all $|\xi_i| = |\eta_i| = 0.5$, and $\beta V = \kappa(L/2)^2 = 0.25\,\kappa \mathrm{L}^2 = 0.25\,\mathrm{L}$,

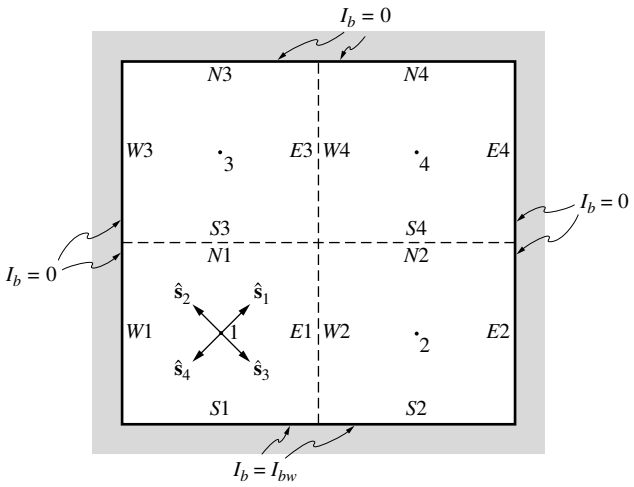

FIGURE 17-4
Square enclosure for Example 17.4.

equation (17.48) becomes

$$I_{pi} = \frac{\frac{1}{8}S_p + \frac{1}{4}I_{x,i} + \frac{1}{4}I_{y,i}}{\frac{1}{8}+\frac{1}{4}+\frac{1}{4}} = \frac{1}{5}\left(S_p + 2I_{x,i} + 2I_{y,i}\right).$$

We start in the lower left corner with all directions for which $\xi_i > 0$ and $\eta_i > 0$ (i.e., a single direction for the S_2-approximation). For this direction x_i = West and y_i = South. To distinguish among the different nodes we attach the node number after the W, etc. For example, $I_{W2,1}$ is the intensity at the West face of volume element 2, pointing into the direction of $\hat{\mathbf{s}}_1$.

$i = 1$ $[\hat{\mathbf{s}}_1 = 0.5(\hat{\mathbf{i}} + \hat{\mathbf{j}})]$: For all nodes

$$\begin{aligned} I_{pj,1} &= \tfrac{1}{5}\left(S_{pj} + 2I_{Wj,1} + 2I_{Sj,1}\right), \\ & I_{Ej,1} = 2I_{pj,1} - I_{Wj,1}, \\ & I_{Nj,1} = 2I_{pj,1} - I_{Sj,1}, \quad j = 1,2,3,4. \end{aligned}$$

Starting at Element 1 we have $I_{W1,1} = 0$, $I_{S1,1} = I_{bw}$, and

$$\begin{aligned} I_{p1,1} &= \tfrac{1}{5}\left(S_{p1} + 2I_{bw}\right), \\ & I_{E1,1} = 2I_{p1,1} = I_{W2,1},\ I_{N1,1} = 2I_{p1,1} - I_{bw} = I_{S3,1}; \\ I_{p2,1} &= \tfrac{1}{5}\left(S_{p2} + 2I_{W2,1} + 2I_{S2,1}\right) = \tfrac{1}{5}\left(S_{p2} + 4I_{p1,1} + 2I_{bw}\right), \\ & I_{N2,1} = 2I_{p2,1} - I_{bw} = I_{S4,1}; \\ I_{p3,1} &= \tfrac{1}{5}\left(S_{p3} + 2I_{S3,1}\right) = \tfrac{1}{5}\left(S_{p3} + 4I_{p1,1} - 2I_{bw}\right), \\ & I_{E3,1} = 2I_{p3,1} = I_{W4,1}; \\ I_{p4,1} &= \tfrac{1}{5}\left(S_{p4} + 2I_{W4,1} + 2I_{S4,1}\right) \\ &= \tfrac{1}{5}\left(S_{p4} + 4I_{p3,1} + 4I_{p2,1} - 2I_{bw}\right). \end{aligned}$$

$i = 2$ $[\hat{\mathbf{s}}_2 = 0.5(-\hat{\mathbf{i}} + \hat{\mathbf{j}})]$: In a problem without symmetry we would start in the lower right corner, scanning again over all elements. However, in this problem we can determine the intensities right away through symmetry, as

$$I_{p1,2} = I_{p2,1},\ I_{p2,2} = I_{p1,1},\ I_{p3,2} = I_{p4,1},\ I_{p4,2} = I_{p3,1}.$$

$i = 3$ $[\hat{\mathbf{s}}_3 = -0.5(\hat{\mathbf{i}} + \hat{\mathbf{j}})]$: Starting in the upper right corner, we have, for all nodes,

$$\begin{aligned} I_{pj,3} &= \tfrac{1}{5}\left(S_{pj} + 2I_{Ej,3} + 2I_{Nj,3}\right), \\ & I_{Wj,3} = 2I_{pj,3} - I_{WE,3}, \\ & I_{Sj,3} = 2I_{pj,3} - I_{Nj,3}. \end{aligned}$$

Starting at Element 4 with $I_{E4,3} = I_{N4,3} = 0$, we find

$$\begin{aligned} & I_{p4,3} = \tfrac{1}{5}S_{p4}, \\ & \qquad I_{S4,3} = 2I_{p4,3} = I_{N2,3},\ I_{W4,3} = 2I_{p4,3} = I_{E3,3}; \\ & I_{p3,3} = \tfrac{1}{5}\left(S_{p3} + 2I_{E3,3}\right) = \tfrac{1}{5}\left(S_{p3} + 4I_{p4,3}\right), \\ & \qquad I_{S3,3} = 2I_{p3,3} = I_{N1,3}; \\ & I_{p2,3} = \tfrac{1}{5}\left(S_{p2} + 2I_{N2,3}\right) = \tfrac{1}{5}\left(S_{p2} + 4I_{p4,3}\right), \\ & \qquad I_{W2,3} = 2I_{p2,3} = I_{E1,3}; \\ & I_{p1,3} = \tfrac{1}{5}\left(S_{p1} + 2I_{E1,3} + 2I_{N1,3}\right) = \tfrac{1}{5}\left(S_{p1} + 4I_{p2,3} + 4I_{p3,3}\right). \end{aligned}$$

Also

$$\begin{aligned} I_{S1,3} &= 2I_{p1,3} - I_{N1,3} = 2(I_{p1,3} - I_{p3,3}), \\ I_{S2,3} &= 2I_{p2,3} - I_{N2,3} = 2(I_{p2,3} - I_{p4,3}), \end{aligned}$$

which will be needed later for the calculation of wall heat fluxes from equation (17.8).

$i = 4$ $[\hat{\mathbf{s}}_4 = 0.5(\hat{\mathbf{i}} - \hat{\mathbf{j}})]$: Again, by symmetry it follows immediately that

$$I_{p1,4} = I_{p2,3},\ I_{p2,4} = I_{p1,3},\ I_{p3,4} = I_{p4,3},\ I_{p4,4} = I_{p3,3},$$

and also

$$I_{S1,4} = I_{S2,3},\ I_{S2,4} = I_{S1,3}.$$

Summarizing, we have

$$\begin{aligned} I_{p1,1} &= I_{p2,2} = \tfrac{1}{5}\left(S_{p1} + 2I_{bw}\right), \\ I_{p2,1} &= I_{p1,2} = \tfrac{1}{5}\left(S_{p2} + 4I_{p1,1} + 2I_{bw}\right), \\ I_{p3,1} &= I_{p4,2} = \tfrac{1}{5}\left(S_{p3} + 4I_{p1,1} - 2I_{bw}\right), \\ I_{p4,1} &= I_{p3,2} = \tfrac{1}{5}\left(S_{p4} + 4I_{p3,1} + 4I_{p2,1} - 2I_{bw}\right), \\ I_{p1,3} &= I_{p2,4} = \tfrac{1}{5}\left(S_{p1} + 4I_{p2,3} + 4I_{p3,3}\right), \\ I_{p2,3} &= I_{p1,4} = \tfrac{1}{5}\left(S_{p2} + 4I_{p4,3}\right), \\ I_{p3,3} &= I_{p4,4} = \tfrac{1}{5}\left(S_{p3} + 4I_{p4,3}\right), \\ I_{p4,3} &= I_{p3,4} = \tfrac{1}{5}S_{p4}, \\ I_{S1,3} &= I_{S2,4} = 2(I_{p1,3} - I_{p3,3}), \\ I_{S2,3} &= I_{S1,4} = 2(I_{p2,3} - I_{p4,3}). \end{aligned}$$

The source functions are readily evaluated from equation (17.7) and symmetry as

$$\begin{aligned} S_{p1} &= S_{p2} = \tfrac{1}{4}(I_{p1,1} + I_{p1,2} + I_{p1,3} + I_{p1,4}), \\ S_{p3} &= S_{p4} = \tfrac{1}{4}(I_{p3,1} + I_{p3,2} + I_{p3,3} + I_{p3,4}). \end{aligned}$$

Since the equations are linear, one could substitute the relations for the S_{pj} into the above equations and solve for the unknown $I_{pj,i}$ by matrix inversion. However, in general one would have many more, and much more complicated, equations, which are best solved by iteration. We start by setting all $S_{pj} = 0$,

TABLE 17.4
Nodal intensities of Example 17.4 as a function of iteration, normalized by I_{bw}.

Iter.	$I_{p1,1}$	$I_{p2,1}$	$I_{p3,1}$	$I_{p4,1}$	$I_{p1,3}$	$I_{p2,3}$	$I_{p3,3}$	$I_{p4,3}$	S_{p1}	S_{p3}
Diamond scheme										
1	0.4000	0.7200	0.0000*	0.1760	0.0000	0.0000	0.0000	0.0000	0.2800	0.0440
2	0.4560	0.8208	0.0000*	0.2654	0.1191	0.0630	0.0158	0.0088	0.3647	0.0725
3	0.4729	0.8513	0.0000*	0.2955	0.1615	0.0846	0.0261	0.0145	0.3926	0.0840
≥9	0.4815	0.8667	0.0037	0.3148	0.1852	0.0963	0.0333	0.0185	0.4074	0.0926
Step scheme										
1	0.3333	0.4444	0.1111	0.1852	0.0000	0.0000	0.0000	0.0000	0.1944	0.0741
2	0.3981	0.5309	0.1574	0.2541	0.1001	0.0730	0.0329	0.0247	0.2755	0.1173
3	0.4252	0.5669	0.1808	0.2883	0.1442	0.1049	0.0521	0.0391	0.3103	0.1401
≥ 10	0.4459	0.5946	0.2027	0.3198	0.1802	0.1306	0.0721	0.0541	0.3378	0.1622

*negative values set to zero

finding values for the $I_{pj,i}$, updating the S_{pj}, reevaluating the $I_{pj,i}$, and so on, until convergence has been reached. The changing values of the intensity (normalized with I_{bw}) as a function of iteration are given in Table 17.4. Values accurate to ≃ 5% are reached after three iterations, and fully converged values (to four significant digits) are obtained after nine iterations. The converged intensities are used to determine the net radiative heat flux from the bottom wall at $x = L/4$ and $x = 3L/4$. From equation (17.8) we have

$$q(x=0.25\,L) = q(x=0.75\,L) = \pi I_{bw} - \sum_{i=3}^{4} w_i\, I_{S1,i}\,|\eta_i| = \pi I_{bw} - \frac{\pi}{2}(I_{S1,3} + I_{S1,4}),$$

or

$$\Psi = \frac{q_{0.25L}}{E_{bw}} = \frac{q_{0.75L}}{E_{bw}} = 1 - \frac{I_{p1,3} - I_{p3,3} + I_{p2,3} - I_{p4,3}}{I_{bw}} = 0.7704.$$

For comparison we will work this example also with the simpler, but more stable step differencing scheme, i.e., $\gamma_x = \gamma_y = 1$. Then we obtain from equations (17.47) and (17.48)

$$I_{pi} = \frac{1}{3}(S_p + I_{x,i} + I_{y,i}), \qquad I_{x,i} = I_{y,i} = I_{pi}.$$

Then, following the same procedure we obtain (a little more easily)

$$I_{p1,1} = \tfrac{1}{3}(S_{p1} + 0 + I_{bw}) = I_{p2,2}$$
$$I_{p2,1} = \tfrac{1}{3}(S_{p2} + I_{p1,1} + I_{bw}) = I_{p1,2}$$
$$I_{p3,1} = \tfrac{1}{3}(S_{p3} + 0 + I_{p1,1}) = I_{p4,2}$$
$$I_{p4,1} = \tfrac{1}{3}(S_{p4} + I_{p3,1} + I_{p2,1}) = I_{p3,2}$$

$$I_{p4,3} = \tfrac{1}{3}(S_{p4} + 0 + 0) = I_{p3,4}$$
$$I_{p3,3} = \tfrac{1}{3}(S_{p3} + I_{p4,3} + 0) = I_{p4,4}$$
$$I_{p2,3} = \tfrac{1}{3}(S_{p2} + 0 + I_{p4,3}) = I_{p1,4}$$
$$I_{p1,3} = \tfrac{1}{3}(S_{p1} + I_{p2,3} + I_{p3,3}) = I_{p2,4}$$

The formulas for the source functions and heat fluxes remain the same, but the nondimensional flux becomes, after substituting for $I_S = I_p$,

$$\Psi = 1 - \frac{I_{p1,3} + I_{p1,4}}{2I_{bw}} = 0.844.$$

The iteration results for the step scheme are also included in Table 17.4. Results for the nondimensional heat flux from both schemes are shown in Fig. 17-5 along with exact results reported by Razzaque and coworkers [59], and with S_2- and S_4-calculations of Truelove [15] (for a much finer mesh). Truelove's results demonstrate the importance of good ordinate sets, at least for low-order approximations: The S_2' and S_4' results were obtained with sets that do not obey the half-moment condition of equation (17.13) (as used by Fiveland [11] in a first investigation of rectangular enclosures), while the S_2 and S_4 results were

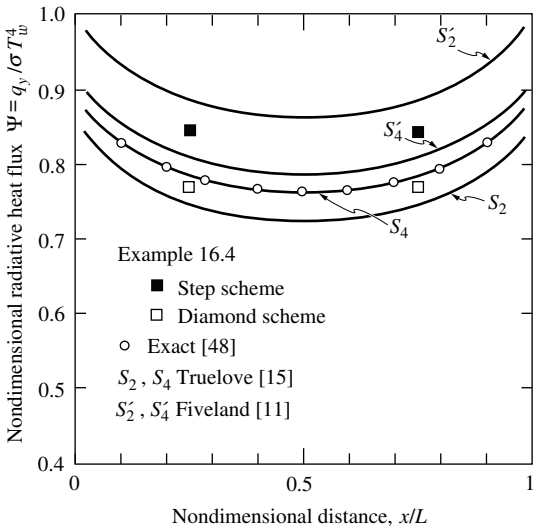

FIGURE 17-5
Nondimensional heat flux along the bottom wall of the square enclosure of Example 17.4.

obtained with the sets given in Table 17.1 (using the nonsymmetric ordinates for S_2). Not surprisingly, the diamond scheme (similar to a Crank–Nicolson finite differencing scheme) is more accurate than the step scheme (similar to fully implicit finite differencing). The step scheme shows a smoother distribution for the I_p and S_p and is always stable. The diamond scheme, on the other hand, gives nonphysical negative intensities for $I_{p3,1}$ during the first few iterations, which were set to zero.

Ray effects, while present, are not apparent in this example because of the large cells used to allow for hand calculations. They become very noticeable when repeating this example with a fine mesh, as will be done in the context of the *finite volume method*, the subject of the next section (see Example 17.7).

In his early calculations Fiveland [11] applied the S_2-, S_4-, and S_6-approximations to purely scattering rectangular media ($\omega = 1$), and to isothermal, nonscattering media bounded by cold black walls. Truelove [15] repeated some of those results to demonstrate the importance of good ordinate sets, and gave some new results for radiative equilibrium in a square enclosure. Jamaluddin and Smith [50] applied the S_4-approximation to a rectangular, nonscattering enclosure with known temperature profile. Kim and Lee investigated the effects of strongly anisotropic scattering, using high-order approximations (up to S_{16}) [60], and the effects of collimated irradiation [61]. Finally, combined conduction and radiation in a linear-anisotropically scattering rectangular enclosure has been studied by Baek and Kim [62]. They also investigated the influence of radiation in compressible, turbulent flow over a backward facing step, using the same method (gray constant properties, here without scattering) [63]. Finally, radiation in two-dimensional packed beds, together with conduction and convection, was studied by Lu and coworkers [36]. While they also assumed gray properties, they allowed them to vary locally; for scattering, they used the large diffuse sphere phase function, equation (12.85). Other applications of the two-dimensional Cartesian form of the discrete ordinates method can be found in [64–67], all dealing with combined-mode heat transfer. Particularly noteworthy here is the study of Selçuk and Kayakol [68], who compared the performance of the S_4 method with that of the related discrete transfer method [69] (see p. 575), finding the methods to have comparable accuracy, while the S_4 solution required three orders of magnitude less computer time.

Three-Dimensional Problems

The method can be extended immediately to three-dimensional geometries by giving the control volume Front and Back surfaces, A_F and A_B, and rewriting equation (17.48) as

$$I_{pi} = \frac{\beta V S_{pi} + |\xi_i| A_x I_{x,i}/\gamma_x + |\eta_i| A_y I_{y,i}/\gamma_y + |\mu_i| A_z I_{z,i}/\gamma_z}{\beta V + |\xi_i| A_{x_e}/\gamma_x + |\eta_i| A_{y_e}/\gamma_y + |\mu_i| A_{z_e}/\gamma_z}, \tag{17.57}$$

where

$$A_x = (1-\gamma_x)\,A_{x_e} + \gamma_x\,A_{x_i}, \tag{17.58a}$$

$$A_y = (1-\gamma_y)\,A_{y_e} + \gamma_y\,A_{y_i}, \tag{17.58b}$$

$$A_z = (1-\gamma_z)\,A_{z_e} + \gamma_z\,A_{z_i}, \tag{17.58c}$$

and the sub-subscript i again denotes the face where the beam enters, and e where it exits, as explained in the context of equation (17.48). A three-dimensional Cartesian enclosure has eight corners, from each of which $\frac{1}{8}N(N+2)$ directions must be traced (covering one *octant* of directions), for a total of $N(N+2)$ ordinates. Some such calculations have been performed by Jamaluddin and Smith [70] (nonscattering medium with prescribed temperature), and by Fiveland [13] and Truelove [16] (both studying the idealized furnace of Mengüç and Viskanta [71], considering a linear-anisotropically scattering medium with internal heat generation at radiative equilibrium), by Park and Yoon [72] (combined conduction and radiation, using inverse analysis to determine constant, gray values for κ and σ_s, for given temperature profiles), and Lacroix and colleagues (radiation in a plasma formed by the laser welding process) [73], and others. Also, Gonçalves and Coelho [74] have shown how the discrete ordinates method can be implemented on parallel computers. Fiveland and Jessee [75] discussed several acceleration schemes for optically thick geometries, for which the discrete ordinate method is known to converge very slowly (or not at all). An extensive review up to the year 2000 of the discrete ordinate method from a computer science point of view, emphasizing convergence rates and multigrid and parallel implementations, has been given by Balsara [76].

Multidimensional Non-Cartesian Geometries

A few investigations have dealt with the application of the discrete ordinates method to two- and three-dimensional cylindrical enclosures, and more recently the method has also been applied to irregular geometries. A two-dimensional axisymmetric enclosure was first considered by Fiveland [10], who calculated radiative heat flux rates for a cylindrical furnace with known temperature profile. A very similar problem was treated by Jamaluddin and Smith [70] who, a little later, also addressed the case of a three-dimensional cylindrical furnace [77,78]. Kim and Baek [79] investigated fully developed nonaxisymmetric pipe flow with a gray, constant property, absorbing/emitting and isotropically scattering medium. Kaplan and coworkers [80] modeled an unsteady ethylene diffusion flame, treating soot and combustion gasses as gray and nonscattering, but with spatial variation. Ramamurthy and colleagues [81] investigated reacting, radiating flow in radiant tubes, using a more sophisticated model for the spectral behavior of the combustion gases, and a molten glass jet was studied by Song and coworkers [82]. All of these used the S_4-method in two-dimensional, cylindrical geometries, although the S_{14}-scheme was used by Jendoubi *et al.* [83] to evaluate different scattering behaviors.

Complex three-dimensional geometries are difficult to treat with the standard discrete ordinates method. This was attempted by Howell and Beckner [84], who used "embedded boundaries" to simulate irregular surfaces, and by Adams and Smith [85], who modeled a complex furnace. Their results clearly demonstrate the ray effect: using a coarse ordinate mesh (up to S_8) together with a very fine spatial mesh, their calculated radiative fluxes undergo very strong unphysical oscillations. Sakami and colleagues [86,87] showed how spatial differentiation can be done across unstructured, triangular, two-dimensional meshes. They trace back each ray through each cell, integrating over the entire cell using a finite-element Galerkin scheme. A somewhat similar approach was suggested by Cheong and Song [88–91]. Through careful spatial differencing, they showed how the standard discrete ordinates method can be applied to unstructured grids and irregular geometries. This method was also further refined by Seo and Kim [92].

Discretization of equation (17.4) for, both, rectangular Cartesian and irregular structured or unstructured grids may also be carried out using the finite volume approach of Patankar [93],

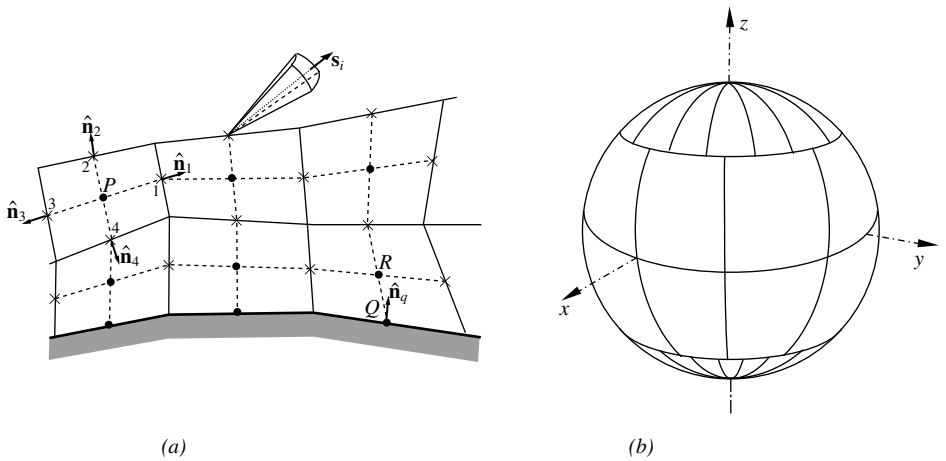

FIGURE 17-6
Spatial and directional discretization in a two-dimensional domain: *(a)* finite volume elements with nodes at the centers of the elements, *(b)* typical subdivision of all directions into solid angle elements.

as is done in the "finite volume method" (for radiation) described in the following section. This can then be combined with any spatial differencing scheme [18]. Alternatively, equation (17.4) can be solved using the finite element approach (e.g., [94,95]), meshless methods (e.g., [96]), etc.

17.6 THE FINITE VOLUME METHOD

The discrete ordinates method, in its standard form, suffers from a number of serious drawbacks, such as false scattering and ray effects. The fact that half-range moments, equation (17.13), must be satisfied for the accurate evaluation of surface fluxes makes it very difficult to apply the method to irregular geometries. Perhaps the most serious drawback of the method is that it does not ensure conservation of radiative energy. This is a result of the fact that the standard discrete ordinates method uses simple quadrature for angular discretization, even though generally a finite volume approach is used for spatial discretization, as outlined in the previous sections. Thus, it was a logical step in the evolution of the method to move to a fully finite volume approach, in space as well as in direction. This was first proposed by Briggs and colleagues [97] in the field of neutron transport. The first formulations for radiative heat transfer were given by Raithby and coworkers [98–101]. Slightly different schemes have been proposed by Chai and colleagues [102–104]. A good review has been given by Raithby [105].

The finite volume method uses exact integration to evaluate solid angle integrals, which is analogous to the evaluation of areas and volumes in the finite volume approach. The method is fully conservative: exact satisfaction of all full- and half-moments can be achieved for arbitrary geometries, and there is no loss of radiative energy. The angular grid can be adapted to each special situation, such as collimated irradiation [102].

Two-Dimensional Formulation

As in the development of the standard discrete ordinates method, for clarity we will limit our development to two-dimensional geometries; extension to three dimensions is straightforward. However, in view of the finite volume method's ability to easily accommodate irregular geometries, we will consider a general two-dimensional domain with irregularly-shaped finite volumes as depicted in Fig. 17-6*a*. The quadrilateral volumes follow "practice B" of Patankar [93], the ones used by Chai and coworkers [104] (i.e., nodes are placed at the center of each finite volume). However, other finite volume schemes may be used, as well. Similar to the spatial domain, the

directional domain of 4π steradians is broken up into n solid angles Ω_i ($i = 1, 2, \ldots, n$), which exactly fill the directional domain without overlap. This can be done in many ways, and without restrictions, but it is usually easiest to define the Ω_i as the areas on a unit sphere defined by lines of longitude and latitude, as shown in Fig. 17-6*b*.

The starting point for the analysis is again equation (17.1) together with its boundary condition, equation (17.2). For each volume element, such as the one surrounding point P in Fig. 17-6*a*, equation (17.1) is integrated over the volume element and over each of the solid angle elements Ω_i. The volume integration over $\partial I/\partial s$ is the same as in equation (17.41), but is now for an element of arbitrary shape, for which we obtain

$$\int_V \frac{\partial I}{\partial s}\, dV = \int_V \hat{\mathbf{s}} \cdot \boldsymbol{\nabla} I\, dV = \int_V \boldsymbol{\nabla} \cdot (\hat{\mathbf{s}} I)\, dV = \int_\Gamma I \hat{\mathbf{s}} \cdot \hat{\mathbf{n}}\, d\Gamma, \tag{17.59}$$

where Γ is the surface of the volume element consisting of four (two-dimensional) or six (three-dimensional) faces and $\hat{\mathbf{n}}$ is the outward surface normal as indicated in the figure. In equation (17.59) the unit direction vector $\hat{\mathbf{s}}$ can be moved inside the spatial $\boldsymbol{\nabla}$-operator since directional coordinates are independent from spatial coordinates. Conversion to a surface integral in the last step follows from the divergence theorem [106].

Thus, integrating equation (17.1) over the volume element V and solid angle Ω_i leads to

$$\int_{\Omega_i} \int_\Gamma I \hat{\mathbf{s}} \cdot \hat{\mathbf{n}}\, d\Gamma\, d\Omega = \int_{\Omega_i} \int_V (\kappa I_b - \beta I)\, dV\, d\Omega + \int_{\Omega_i} \int_V \frac{\sigma_s}{4\pi} \int_{4\pi} \Phi(\hat{\mathbf{s}}', \hat{\mathbf{s}}) I(\hat{\mathbf{s}}')\, d\Omega'\, dV\, d\Omega. \tag{17.60}$$

In the simplest implementation of the finite volume method it is assumed, for the term on the left-hand side, that the intensity is constant across each face of the element as well as over the solid angle Ω_i. Similarly, it is assumed for the volume integrals that values are constant throughout and equal to the value at point P. Equation (17.60) then becomes

$$\sum_k I_{ki}(\mathbf{s}_i \cdot \hat{\mathbf{n}}_k) A_k = \beta_p (S_{pi} - I_{pi}) V \Omega_i, \tag{17.61a}$$

$$S_{pi} = (1 - \omega_p) I_{bp} + \frac{\omega_p}{4\pi} \sum_{j=1}^{n} I_{pj} \bar{\Phi}_{ij}, \tag{17.61b}$$

$$\bar{\Phi}_{ij} = \frac{1}{\Omega_i} \int_{\Omega_i} \int_{\Omega_j} \Phi(\hat{\mathbf{s}}', \hat{\mathbf{s}})\, d\Omega'\, d\Omega, \tag{17.61c}$$

$$\mathbf{s}_i = \int_{\Omega_i} \hat{\mathbf{s}}\, d\Omega, \tag{17.61d}$$

where subscripts k and p imply evaluation at the center of the volume's faces A_k (as indicated by an $\times$ in Fig. 17-6*a)* and element center P, respectively; subscript i denotes a value associated with solid angle Ω_i. The radiative source S_{pi} is similar to the one in equation (17.39), but now has an analytically averaged phase function $\bar{\Phi}_{ij}$. Finally, the $\mathbf{s}_i$ is a vector (of varying length indicative of the size of Ω_i) pointing into an average direction within solid angle element Ω_i. Of course, the forward-scattering term in S_{pi} can, and should, be removed as was done in the standard discrete ordinate formulation [cf. equation (17.50)].

What remains to be done is to relate the intensities at the face centers, I_{ki}, to those at volume centers, I_{pi}. There are many different ways to do this. Raithby and coworkers [98], in particular, have developed schemes of high accuracy. However, such sophisticated schemes require substantial analytical and computational overhead. In light of the stability considerations discussed by Chai and colleagues [48], the simple step scheme has generally been preferred. Therefore, similar to equation (17.43) with $\gamma = 1$, we assume that for intensities *leaving* control volume P (i.e., for $\mathbf{s}_i \cdot \hat{\mathbf{n}}_k > 0$) $I_{ki} = I_{pi}$. All *incoming* intensities ($\mathbf{s}_i \cdot \hat{\mathbf{n}}_k < 0$) are assigned the value of the

element center from which they came. Substituting $I_{ki} = I_{pi}$ for $\mathbf{s}_i \cdot \hat{\mathbf{n}}_k > 0$ into equation (17.61) then leads to the final expression

$$I_{pi} = \frac{\beta_p S_{pi} V \Omega_i + \sum\limits_{k,\text{in}} I_{ki} \left|\mathbf{s}_i \cdot \hat{\mathbf{n}}_k\right| A_k}{\beta_p V \Omega_i + \sum\limits_{k,\text{out}} (\mathbf{s}_i \cdot \hat{\mathbf{n}}_k) A_k}, \tag{17.62}$$

where the "in" and "out" on the summation signs denote summation over volume faces with incoming ($\mathbf{s}_i \cdot \hat{\mathbf{n}}_k < 0$) or outgoing ($\mathbf{s}_i \cdot \hat{\mathbf{n}}_k > 0$) intensities, only. Lately, the CLAM scheme has become popular (e.g., [58, 107]), requiring an iterative approach as discussed in Section 17.5.

The boundary conditions are developed in a similar manner, except that—for diffusely emitting and reflecting surfaces—it is advantageous to make an energy balance to ensure conservation of radiative energy for surfaces not lined up with the solid angles Ω_i. Multiplying equation (17.2) by $\hat{\mathbf{n}} \cdot \hat{\mathbf{s}}$ and integrating over all outgoing directions gives an expression for surface radiosity as

$$J_w = \int\limits_{\hat{\mathbf{n}}\cdot\hat{\mathbf{s}}>0} I\, \hat{\mathbf{n}} \cdot \hat{\mathbf{s}}\, d\Omega = \int\limits_{\hat{\mathbf{n}}\cdot\hat{\mathbf{s}}>0} \epsilon_w I_{bw}\, \hat{\mathbf{n}} \cdot \hat{\mathbf{s}}\, d\Omega + (1-\epsilon_w) \int\limits_{\hat{\mathbf{n}}\cdot\hat{\mathbf{s}}<0} I\, |\hat{\mathbf{n}} \cdot \hat{\mathbf{s}}|\, d\Omega. \tag{17.63}$$

In finite volume form, integrating over a surface element such as A_Q shown in Fig. 17-6*a*, and making the standard assumption of constant intensities across A_Q leads to

$$I_{q0} \sum_{i,\text{out}} \mathbf{s}_i \cdot \hat{\mathbf{n}}_q\, A_Q = \epsilon_q I_{bq} \sum_{i,\text{out}} \mathbf{s}_i \cdot \hat{\mathbf{n}}_q\, A_Q + (1-\epsilon_q) \sum_{i,\text{in}} I_{qi} \left|\mathbf{s}_i \cdot \hat{\mathbf{n}}_q\right| A_Q \tag{17.64}$$

or

$$I_{q0} = \epsilon_q I_{bq} + (1-\epsilon_q) \sum_{i,\text{in}} I_{qi} \left|\mathbf{s}_i \cdot \hat{\mathbf{n}}_q\right| \Big/ \sum_{i,\text{out}} (\mathbf{s}_i \cdot \hat{\mathbf{n}}_q), \tag{17.65}$$

where I_{q0} is the diffuse intensity leaving boundary element Q (same for all outgoing directions Ω_i with $\mathbf{s}_i \cdot \hat{\mathbf{n}}_k > 0$), $\hat{\mathbf{n}}_q$ is the unit surface normal at Q pointing *out* of the boundary (but *into* the adjacent volume element R). The I_{qi} are intensities leaving the adjacent volume element R going into boundary element Q. Using the step scheme we can set $I_{qi} = I_{Ri}$ for $\mathbf{s}_i \cdot \hat{\mathbf{n}}_q < 0$.

Once all internal intensities I_{pi} and boundary intensities I_{qi} have been determined, internal values for incident radiation and radiative flux are found from

$$G_p = \sum_i I_{pi} \Omega_i, \qquad \mathbf{q}_p = \sum_i I_{pi} \mathbf{s}_i, \tag{17.66}$$

while wall fluxes are given by

$$q_q = \epsilon_q \left(E_{bq} - H_q\right) = \epsilon_q \left(I_{bq} \sum_{i,\text{out}} \mathbf{s}_i \cdot \hat{\mathbf{n}}_q - \sum_{i,\text{in}} I_{qi} \left|\mathbf{s}_i \cdot \hat{\mathbf{n}}_q\right| \right). \tag{17.67}$$

Note that, for arbitrarily oriented surfaces, the sums of $|\mathbf{s}_i \cdot \hat{\mathbf{n}}_q|$ may not add up to π (for either incoming or outgoing directions); therefore, for consistency, the finite volume rendition for E_{bq} given in the right-most part of equation (17.67) is preferred.

Example 17.5. Repeat Example 17.1 for the finite volume method, using the upper and lower hemispheres as solid angle ranges.

Solution

The governing equation is, as before,

$$\mu \frac{dI}{d\tau} + I = (1-\omega)\, I_b + \frac{\omega}{4\pi} (G + A_1\, q\mu).$$

If we want to apply the finite volume method in a similar fashion as in Example 17.1, i.e., to obtain a differential equation for each solid angle range, then we need only integrate the governing equation

over these solid angles, not over volume. Assuming a constant intensity I^+ over the upper hemisphere, and I^- over the lower one, we obtain with $I_b = G/4\pi$

$$\text{upper hemisphere: } \int_0^{2\pi}\int_0^1 \left[\mu\frac{dI^+}{d\tau} + I^+ = \frac{1}{4\pi}(G + A_1\omega\mu q)\right] d\mu\, d\psi,$$
$$\text{lower hemisphere: } \int_0^{2\pi}\int_{-1}^0 \left[\mu\frac{dI^-}{d\tau} + I^- = \frac{1}{4\pi}(G + A_1\omega\mu q)\right] d\mu\, d\psi,$$

or

$$\pi\frac{dI^+}{d\tau} + 2\pi I^+ = \frac{1}{2}G + \frac{1}{4}A_1\omega q,$$
$$-\pi\frac{dI^-}{d\tau} + 2\pi I^- = \frac{1}{2}G - \frac{1}{4}A_1\omega q.$$

From the definitions for heat flux and incident radiation we have again

$$\begin{Bmatrix} G \\ q \end{Bmatrix} = \int_0^{2\pi}\int_{-1}^{+1} \begin{Bmatrix} 1 \\ \mu \end{Bmatrix} I\, d\mu\, d\psi = \begin{Bmatrix} 2\pi\,(I^+ + I^-) \\ \pi\,(I^+ - I^-) \end{Bmatrix},$$

as in Example 17.1. Thus adding and subtracting the equations for the upper and lower hemispheres we obtain

$$\frac{dq}{d\tau} + G = G \qquad \text{or} \quad \frac{dq}{d\tau} = 0,$$
$$\frac{1}{2}\frac{dG}{d\tau} + 2q = \frac{1}{2}A_1\omega q \quad \text{or} \quad \frac{dG}{d\tau} = -(4 - A_1\omega)\, q.$$

For the boundary conditions, equation (17.65), we need to first calculate the $\mathbf{s}_i$:

$$\mathbf{s}_1 = \int_0^{2\pi}\int_0^{\pi/2} (\sin\theta\cos\psi\hat{\mathbf{i}} + \sin\theta\sin\psi\hat{\mathbf{j}} + \cos\theta\hat{\mathbf{k}})\sin\theta\, d\theta\, d\psi = \pi\hat{\mathbf{k}},$$
$$\mathbf{s}_2 = \int_0^{2\pi}\int_{\pi/2}^{\pi} (\sin\theta\cos\psi\hat{\mathbf{i}} + \sin\theta\sin\psi\hat{\mathbf{j}} + \cos\theta\hat{\mathbf{k}})\sin\theta\, d\theta\, d\psi = -\pi\hat{\mathbf{k}}.$$

For the bottom boundary we have $\hat{\mathbf{n}} = \hat{\mathbf{k}}$ and $\mathbf{s}_1 \cdot \hat{\mathbf{n}} = -\mathbf{s}_2 \cdot \hat{\mathbf{n}} = \pi$, so that at

$$\tau = 0: \qquad I^+ = \epsilon_1 I_{b1} + (1 - \epsilon_1)I^-.$$

Subtracting $(1 - \epsilon_1)I^+$, using the definition for q, and dividing by ϵ_1 leads to

$$\tau = 0: \qquad I^+ = J_1/\pi = I_{b1} - \frac{1 - \epsilon_1}{\epsilon_1\pi}q,$$

which is, of course, the same as for Example 17.1 (and for any diffuse surface). Similarly, at the top wall

$$\tau = \tau_L: \qquad I^- = J_2/\pi.$$

The solution is then found immediately from Example (17.1) (setting $1/\mu_1^2 = 4$) as

$$\Psi = \frac{q}{J_1 - J_2} = \frac{1}{1 + \left(1 + \frac{A_1\omega}{4}\right)\tau_L},$$

which is the same as the answer from the nonsymmetric S_2-approximation. More importantly, the analysis in this example shows that the Schuster–Schwarzschild (or two-flux) approximation is simply the lowest-level finite volume method.

Example 17.6. Repeat Example 17.4 using the finite volume method, by splitting the total solid angle into four equal ranges.

Solution

As in Example 17.4 we will put the z-axis perpendicular to the paper in Fig. 17-4, from which the polar angle θ is measured. Because of the two-dimensionality, it is best to assign each Ω_i the entire range of

polar angles, and a quarter of the azimuthal range. Thus, breaking up by quadrant we choose

$$\begin{aligned}
\Omega_1: &\qquad 0 \le \psi < \frac{\pi}{2}, &\qquad 0 \le \theta \le \pi,\\
\Omega_2: &\qquad \frac{\pi}{2} \le \psi < \pi, &\qquad 0 \le \theta \le \pi,\\
\Omega_3: &\qquad \pi \le \psi < \frac{3\pi}{2}, &\qquad 0 \le \theta \le \pi,\\
\Omega_4: &\qquad \frac{3\pi}{2} \le \psi < 2\pi, &\qquad 0 \le \theta \le \pi.
\end{aligned}$$

The solid angle vectors $\mathbf{s}_i$ are obtained with $\hat{\mathbf{s}} = \sin\theta\cos\psi\hat{\mathbf{i}} + \sin\theta\sin\psi\hat{\mathbf{j}} + \cos\theta\hat{\mathbf{k}}$ as

$$\begin{aligned}
\mathbf{s}_i &= \int_{\Delta\psi_i}\int_0^{\pi} \hat{\mathbf{s}}\sin\theta\, d\theta\, d\psi = \int_{\Delta\psi_i}\left[\frac{\pi}{2}\cos\psi\hat{\mathbf{i}} + \frac{\pi}{2}\sin\psi\hat{\mathbf{j}} + 0\hat{\mathbf{k}}\right] d\psi\\
&= \left(\frac{\pi}{2}\sin\psi\hat{\mathbf{i}} - \frac{\pi}{2}\cos\psi\hat{\mathbf{j}}\right)\Big|_{\Delta\psi_i},
\end{aligned}$$

or

$$\mathbf{s}_1 = \frac{\pi}{2}(\hat{\mathbf{i}}+\hat{\mathbf{j}}), \quad \mathbf{s}_2 = -\frac{\pi}{2}(\hat{\mathbf{i}}-\hat{\mathbf{j}}), \quad \mathbf{s}_3 = -\frac{\pi}{2}(\hat{\mathbf{i}}+\hat{\mathbf{j}}), \quad \mathbf{s}_4 = \frac{\pi}{2}(\hat{\mathbf{i}}-\hat{\mathbf{j}}),$$

which are identical to the directions in Example 17.4, except for the factor π (which gives the total solid angle of the Ω_i), and the fact that the $\hat{\mathbf{s}}_i$ in Example 17.4 were *projections* in the x-y-plane, while the $\mathbf{s}_i$ in this example actually *lie* in the x-y-plane. Now, with $A_k = \frac{1}{2}L$, $\beta V = \kappa\left(\frac{1}{2}L\right)^2 = \frac{1}{4}L$, and $\Omega_i = \pi$, we obtain from equation (17.62)

$$\Omega_1\ (i=1): \quad I_{p1} = \frac{\frac{1}{4}L\pi S_{p1} + I_{W1}\left|\mathbf{s}_1\cdot(-\hat{\mathbf{i}})\right|\frac{1}{2}L + I_{S1}\left|\mathbf{s}_1\cdot(-\hat{\mathbf{j}})\right|\frac{1}{2}L}{\frac{1}{4}L\pi + \mathbf{s}_1\cdot\hat{\mathbf{i}}\,\frac{1}{2}L + \mathbf{s}_1\cdot\hat{\mathbf{j}}\,\frac{1}{2}L}, \ p = 1,2,3,4,$$

and similarly for the other three directions. Evaluating the dot products and simplifying this may be written in general form for all nodes and all directions as

$$I_{pi} = \frac{1}{3}(S_p + I_{px_i,i} + I_{py_i,i}), \quad p,i = 1,2,3,4,$$

where $I_{px_i,i}$ is the intensity entering volume p across the x = const face in the $\mathbf{s}_i$ direction, and similarly for $I_{py_i,i}$. Thus

$$\begin{aligned}
I_{p1,1} &= \frac{1}{3}(S_{p1} + I_{W1,1} + I_{S1,1}) = \frac{1}{3}(S_{p1} + 0 + I_{bW}),\\
I_{p2,1} &= \frac{1}{3}(S_{p2} + I_{W2,1} + I_{S2,1}) = \frac{1}{3}(S_{p2} + I_{p1,1} + I_{bW}),\\
&\dots,
\end{aligned}$$

which is exactly the same as the S_2-approximation together with the step scheme. This is to be expected since *(i)* the finite volume method—as applied here—uses the step scheme, and *(ii)* the S_2-approximation satisfies all half-moments for this very simple case. The strength of the finite volume method lies in the fact that it is easily applied to irregular geometries, and that it conserves radiative energy. As in Example 17.4 ray effects are not obvious because of the coarse spatial mesh.

Appendix F includes program `FVM2D.f`, developed by Chai and colleagues [102–104], which solves equations (17.62), (17.65) and (17.67) for arbitrary rectangular enclosures.

Example 17.7. Repeat Example 17.6 using program `FVM2D.f` to allow for fine grid and ordinate resolution. In particular, consider the case where only a part of the bottom strip, $-0.1 < x < +0.1$, is heated.

Solution

As in Example 17.4 we will put the z-axis perpendicular to the paper. We will use $N \times N$ cells in the x-y-plane, and discretize the total solid angle into $4 \times M$ subangles, limiting ourselves to 4 polar angles because of the two-dimensional nature of the problem. Results obtained by `FVM2D.f` for irradiation

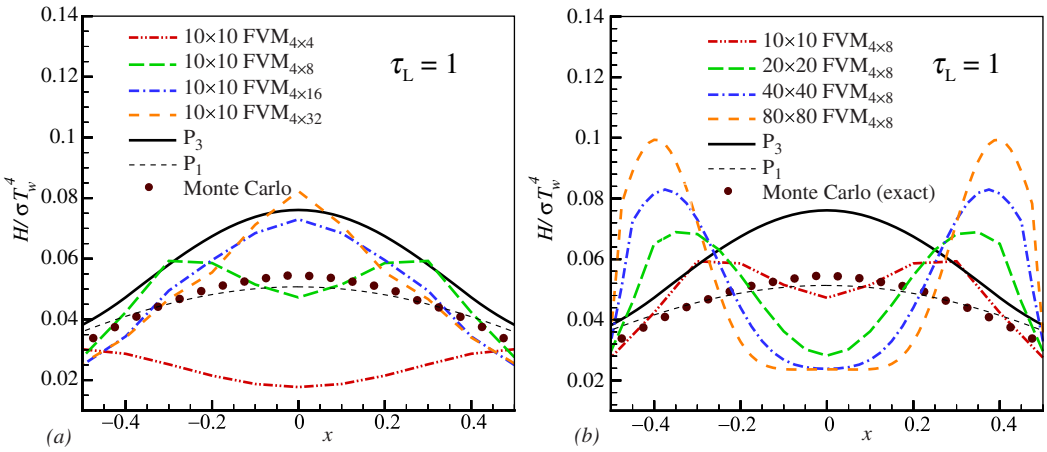

FIGURE 17-7
Irradiation of top surface in a square enclosure with heated strip at bottom wall: *(a)* effects of directional discretization, *(b)* effects of spatial discretization.

upon the top surface, for an optically intermediate case of $\tau_L = \kappa L = 1$, are shown in Fig. 17-7. The answers are compared with exact results from the Monte Carlo method (see Chapter 21), and also with those obtained from the P_1- and P_3-approximations described in the previous chapter. Note that, for radiative equilibrium of a gray medium with isotropic scattering, the solution only depends on extinction coefficient (regardless of what fraction is scattered or absorbed/reemitted), and the present example is identical to the case presented in Fig. 16-11 (except for the partially heated strip considered here). Figure 17-7*a* shows the effects of directional discretization for a fixed 10×10 spatial grid. It is observed that accuracy improves as we go from 4×4 to 4×8 directions, but deteriorates for much finer directional spacing. Ray effects are even more obvious in Fig. 17-7*b* for a fixed directional discretization of 4×8: as the spatial grid becomes finer, more and more cells away from the heated wall receive no direct radiation along the chosen ordinates. Clearly, for a (relatively coarse) 4×8 directional discretization a (coarse) 10×10 spatial grid gives the most accurate answer, with rapidly diminishing accuracy for finer grids. Note that in the finite volume approach ray effects are *less* pronounced than in the standard discrete ordinates method (with its discrete directions as opposed to averaged solid angles), which is therefore expected to perform even worse for the present case.

In comparison, the P_N answers are relatively accurate, because they do not suffer from ray effects, and their answers are independent of spatial discretization (beyond a minimum $N \times N$ discretization to avoid noticeable truncation errors). In this particular example, P_1 actually outperforms P_3. This does not mean that the P_N-approximations are superior to the discrete ordinates approach, (or that P_1 is better than P_3), as seen from the additional results given in Fig. 16-11 and the direct comparison between P_N and FVM given in [108] for this and several other problems.

Murthy and Mathur [109–111] pointed out that, in general, equations (17.62), (17.65), and (17.67) incur errors due to solid angle overhang. For example, for face k of volume element P part of solid angle Ω_i with $\mathbf{s}_i \cdot \hat{\mathbf{n}}_k > 0$ (pointing out of volume element) may actually overlap *into* the element. Similarly, it is unlikely to have solid angle boundaries lined up perfectly with the solid boundaries everywhere. They improved the accuracy of the method through pixelation, i.e., by breaking up Ω_i into smaller pieces, to determine overlap fractions. Also, noting that the standard line iteration method leads to unacceptably slow convergence in optically thick situations, they introduced a new scheme, which updates all directional intensities within a cell simultaneously, leading to convergence rates essentially independent of optical thickness [111,112]. Hassanzadeh and coworkers [113] also developed a method to accelerate convergence for optically thick media by carrying out iterations in terms of mean intensity, $G/4\pi$, as opposed to all directional intensities. Several other improvements to the method have been suggested. Kim and Huh [114] noted that most researchers broke up the total solid angle of 4π into $N \times N$

segments of equal polar angles θ and azimuthal angles ψ. This makes the Ω_i very small near the poles ($\theta = 0, \pi$), and large near the equator ($\theta = \pi/2$). They suggest that, for n different polar angles θ_i, one should pick fewer azimuthal angles near the poles, namely a distribution of $4, 8, ..., 2n-4, 2n, 2n, 2n-4, ..., 8, 4$ with growing θ_i. This results in $n(n+2)$ different solid angles (equal to the number of ordinates in the standard S_n scheme), with all Ω_i being roughly equally large. Finally, Liu and coworkers [115] have shown how the finite volume method with unstructured grids can be parallelized using domain decomposition. The method has also been employed in a number of combined heat transfer problems [116,117] and is included in several important commercial CFD codes, such as FLUENT [118].

Comparison with Standard Discrete Ordinates Method

The radiative transfer equation (RTE), equation (17.1), is a five-dimensional integro-differential equation, with three spatial and two directional coordinates. For a numerical solution both, spatial and directional dependencies must be discretized. Various methods of discretization are available, such as finite differences, finite volumes, finite elements, etc., and one or the other may be applied for the spatial and for the directional discretization. Originally, for the standard discrete ordinates method finite differences were used for both. As the method has evolved to more general geometries, different spatial discretization schemes have been employed, but directional discretization has remained in finite difference form. In contrast, in the original form of the finite volume method finite volumes were used for both spatial and directional discretization. However, recently other spatial discretization schemes have also been used, e.g., Cui and Li [119] and Grissa *et al.* [120] employed the finite element method. Therefore, the one defining difference between the standard discrete ordinates method and the finite volume method is the fact that the standard discrete ordinates method uses finite differences for directional discretization, while the finite volume method employs finite volumes.

Liu and coworkers [121] have expressed the RTE in general boundary-fitted coordinates [122], and applied both the standard discrete ordinates method and the finite volume method to a number of two- and three-dimensional problems. They found both methods to require similar amounts of CPU time, while the finite volume method was always slightly more accurate. Similar conclusions were drawn by Fiveland and Jessee [123] and by Kim and Huh [124], noting that the finite volume (FV) method outperforms standard discrete ordinates particularly in optically thin media, since it is less sensitive to ray effects. Coelho and coworkers [125] compared the performance of the FV method with that of the discrete transfer method [69] and, like Selçuk and Kayakol [68], found the FV method to be much more economical. Major advantages of the finite volume method are greater freedom to select ordinates, and the fact that the FV method conserves radiative energy. In addition, treatment of complex enclosures comes more natural to the FV method. For example, Baek and colleagues [126–128] used boundary-fitted coordinates to investigate radiation in several three-dimensional enclosures with gray, constant-property media.

17.7 THE MODIFIED DISCRETE ORDINATES METHOD

It was noted in Section 17.5 that the discrete ordinates method (in its standard or finite volume form) can suffer from ray effects, if directional discretization is coarse compared to spatial discretization, and if the medium contains small sources of strong emission (from walls or from within the medium). This prompted Ramankutty and Crosbie [129,130] to separate boundary emission from medium emission, as is done in the modified differential approximation of Section 16.8, i.e., letting

$$I(\mathbf{r}, \hat{\mathbf{s}}) = I_w(\mathbf{r}, \hat{\mathbf{s}}) + I_m(\mathbf{r}, \hat{\mathbf{s}}). \tag{17.68}$$

The wall-related intensity field can be solved by any standard method as outlined in Section 17.5, while the RTE and boundary conditions for I_m become

$$\frac{dI_m}{ds} = \kappa I_b - \beta I_m(\hat{\mathbf{s}}) + \frac{\sigma_s}{4\pi}\int_{4\pi} I_m(\hat{\mathbf{s}}')\,\Phi(\hat{\mathbf{s}}',\hat{\mathbf{s}})\,d\Omega' + \frac{\sigma_s}{4\pi}\int_{4\pi} I_w(\hat{\mathbf{s}}')\,\Phi(\hat{\mathbf{s}}',\hat{\mathbf{s}})\,d\Omega', \tag{17.69}$$

$$I_m(\mathbf{r}_w,\hat{\mathbf{s}}) = \frac{1-\epsilon}{\pi}\int_{\hat{\mathbf{n}}\cdot\hat{\mathbf{s}}'<0} I_m\hat{\mathbf{s}}')\,|\hat{\mathbf{n}}\cdot\hat{\mathbf{s}}'|\,d\Omega'. \tag{17.70}$$

Again, equations (17.69) and (17.70) are valid for a gray medium or, on a spectral basis, for a nongray medium, in an enclosure with opaque, diffusely emitting and diffusely reflecting walls. Comparing with equations (17.4) and (17.5) it is apparent that the modified equation for I_m can be solved in the same manner by replacing the emission term, κI_b, in equation (17.4) by

$$\kappa\, I_b + \frac{\sigma_s}{4\pi}\sum_{j=1}^{n} w_j\, I_w(\hat{\mathbf{s}}_j)\,\Phi(\hat{\mathbf{s}}_j,\hat{\mathbf{s}}_i).$$

For a given temperature and radiative property field the wall-related intensity is calculated once and for all, and does not require reevaluation during the iterations required for I_m in the presence of scattering, wall reflections, or higher-order spatial schemes. Alternatively, equations (17.69) and (17.70) can also be solved with the finite volume method by adding the I_w-related scattering source to S_{pi} in equation (17.61*b*). Ramankutty and Crosbie applied the modified discrete ordinates method to boundary-emission dominated rectangular enclosures with black walls, using analytical solutions for I_w. For such problems, when using lower-order S_N-techniques with fine spatial meshes, the standard discrete ordinates method shows strong ray effects, which are completely mitigated by the modified discrete ordinates approach. Sakami and colleagues [131, 132] and Baek and coworkers [128, 133] investigated irregular geometries with this *modified discrete ordinates method*, the latter employing a straightforward Monte Carlo scheme for the wall emission part, giving excellent accuracy even with extreme boundary source terms.

However, like the modified differential approximation, the modified discrete ordinates method cannot improve the accuracy of the underlying standard method if strong, isolated emission sources are located *within* the medium. Coelho [56] and Li and Werther [134] extended the method by associating all emission (walls and medium) with I_w, and only scattered radiation is calculated by discrete ordinates. While this mitigates all ray effects, it is not clear what is gained by this approach (since solution for the emission-related intensity is essentially as involved as the full problem).

17.8 EVEN-PARITY FORMULATION

The directional RTEs that are solved for the standard discrete ordinates method, equation (17.4), or the finite volume method, equation (17.61), are first-order partial differential equations with hyperbolic character, which can lead to unphysical results (negative intensities) and may display strong ray effects. Converting them into second-order boundary value problems eliminates unphysical results and could potentially mitigate ray effects. In the heat transfer field this was first attempted by Song and Park [135]. A second-order formulation may be obtained by defining even- and odd-parity intensities, involving both forward $\hat{\mathbf{s}}$ and backward $-\hat{\mathbf{s}}$ directions along a line:

$$\psi(\mathbf{r},\hat{\mathbf{s}}) = I(\mathbf{r},\hat{\mathbf{s}}) + I(\mathbf{r},-\hat{\mathbf{s}}), \tag{17.71}$$

$$\phi(\mathbf{r},\hat{\mathbf{s}}) = I(\mathbf{r},\hat{\mathbf{s}}) - I(\mathbf{r},-\hat{\mathbf{s}}). \tag{17.72}$$

In the following discussion we will limit ourselves to the simpler case of isotropic scattering. Under those conditions, adding and subtracting the RTE (17.1) for both directions $\hat{\mathbf{s}}$ and $-\hat{\mathbf{s}}$ leads to

$$\hat{\mathbf{s}} \cdot \nabla\phi(\mathbf{r}, \hat{\mathbf{s}}) = -\beta(\mathbf{r})\psi(\mathbf{r}, \hat{\mathbf{s}}) + 2\kappa(\mathbf{r})\, I_b(\mathbf{r}) + \frac{2\sigma_s(\mathbf{r})}{4\pi} \int_{2\pi} \psi(\mathbf{r}, \hat{\mathbf{s}}')\, d\Omega', \tag{17.73}$$

$$\hat{\mathbf{s}} \cdot \nabla\psi(\mathbf{r}, \hat{\mathbf{s}}) = -\beta(\mathbf{r})\phi(\mathbf{r}, \hat{\mathbf{s}}). \tag{17.74}$$

Note that integration over all directions now encompasses only 2π (half a unit sphere). Using equation (17.74) the odd-parity term is easily eliminated, leading to a parabolic, second-order partial differential equation,

$$\hat{\mathbf{s}} \cdot \nabla\left(\frac{1}{\beta(\mathbf{r})}\hat{\mathbf{s}} \cdot \nabla\psi(\mathbf{r}, \hat{\mathbf{s}})\right) = \beta(\mathbf{r})\psi(\mathbf{r}, \hat{\mathbf{s}}) - 2\kappa(\mathbf{r})\, I_b(\mathbf{r}) - \frac{2\sigma_s(\mathbf{r})}{4\pi} \int_{2\pi} \psi(\mathbf{r}, \hat{\mathbf{s}}')\, d\Omega', \tag{17.75}$$

which requires a boundary condition at each end (boundary intersection) of the dual-direction ray. Substituting equations (17.71) and (17.72) into (17.2) gives

$$\psi(\mathbf{r}_w, \hat{\mathbf{s}}) + \phi(\mathbf{r}_w, \hat{\mathbf{s}}) = 2\epsilon(\mathbf{r}_w) I_b(\mathbf{r}_w) + \frac{\rho(\mathbf{r}_w)}{\pi} \int_{\hat{\mathbf{n}}\cdot\hat{\mathbf{s}}'<0} [\psi(\mathbf{r}_w, \hat{\mathbf{s}}') - \phi(\mathbf{r}_w, \hat{\mathbf{s}}')]\, |\hat{\mathbf{n}} \cdot \hat{\mathbf{s}}'|\, d\Omega', \quad \hat{\mathbf{n}} \cdot \hat{\mathbf{s}} > 0. \tag{17.76}$$

Because of the dual-directional nature of ψ and ϕ, the boundary condition must also be applied in the $-\hat{\mathbf{s}}$-direction, or

$$\psi(\mathbf{r}_w, \hat{\mathbf{s}}) - \phi(\mathbf{r}_w, \hat{\mathbf{s}}) = 2\epsilon(\mathbf{r}_w) I_b(\mathbf{r}_w) + \frac{\rho(\mathbf{r}_w)}{\pi} \int_{\hat{\mathbf{n}}\cdot\hat{\mathbf{s}}'<0} [\psi(\mathbf{r}_w, \hat{\mathbf{s}}') + \phi(\mathbf{r}_w, \hat{\mathbf{s}}')]\, |\hat{\mathbf{n}} \cdot \hat{\mathbf{s}}'|\, d\Omega', \quad \hat{\mathbf{n}} \cdot \hat{\mathbf{s}} < 0. \tag{17.77}$$

These two differ only with the sign of $\hat{\mathbf{n}} \cdot \hat{\mathbf{s}}$; they are readily combined and ϕ is eliminated giving the proper boundary conditions at both ends of a ray described by equation (17.75) as

$$\begin{aligned} &\psi(\mathbf{r}_w, \hat{\mathbf{s}}) - \operatorname{sign}(\hat{\mathbf{n}} \cdot \hat{\mathbf{s}}) \frac{1}{\beta(\mathbf{r})} \hat{\mathbf{s}} \cdot \nabla\psi(\mathbf{r}, \hat{\mathbf{s}}) \\ &\quad = 2\epsilon(\mathbf{r}_w) I_b(\mathbf{r}_w) + \frac{\rho(\mathbf{r}_w)}{\pi} \int_{\hat{\mathbf{n}}\cdot\hat{\mathbf{s}}'<0} \left[\psi(\mathbf{r}_w, \hat{\mathbf{s}}') + \operatorname{sign}(\hat{\mathbf{n}} \cdot \hat{\mathbf{s}}) \frac{1}{\beta(\mathbf{r})} \hat{\mathbf{s}} \cdot \nabla\psi(\mathbf{r}, \hat{\mathbf{s}}')\right] |\hat{\mathbf{n}} \cdot \hat{\mathbf{s}}'|\, d\Omega'. \end{aligned} \tag{17.78}$$

In the even-parity formulation directional discretization is only over 2π or a half-sphere, i.e., only half as many ordinates are required and, instead, second-order partial differential equations need to be solved. Spatial discretization may be done by central differences [135], by finite volumes [136,137], or by finite elements [94,123,138,139]; directional discretization has generally been done according to the standard discrete ordinates method, with the exception of Becker and coworkers [139], who employed finite elements also for directional discretization. Liu *et al.* [137], Fiveland and Jessee [123], and Kang and Song [138] compared the standard implementation of the discrete ordinates method to the even-parity formulation and found, in general, that the accuracy was similar, but the even-parity model required more CPU time, particularly in optically thin situations.

17.9 OTHER RELATED METHODS

The difficulty caused by the directional nature of radiation has prompted a number of researchers to develop various approximate schemes to discretize directions (similar to the standard discrete ordinates method) or to average over solid angle ranges (akin to the finite volume method). We will here briefly discuss the most important of these related models.

Flux Methods. We have already seen in Example 17.5 that the two-flux or Schuster–Schwarzschild approximation is nothing but a crude implementation of the finite volume method. The

two-flux method has been applied to one-dimensional problems by a number of investigators, usually in situations where the accurate determination of radiative fluxes is not crucial [140–145]. Noting that the accuracy of this method is more or less limited to one-dimensional problems without anisotropic scattering, Chin and Churchill [146, 147] developed the six-flow method, primarily to deal with strongly anisotropic scattering in the presence of collimated irradiation. In this method the intensity is broken up into a forward, a backward, and four (usually equal) sideways components. How these components are broken up or averaged over the total solid angle of 4π is arbitrary. The method has been applied by various researchers to several two- and three-dimensional problems [147–150].

Discrete Transfer Method. The discrete transfer method (DTM) was developed by Lockwood and Shah [69], several years before serious development of the discrete ordinates method (DOM) began. The discrete transfer method is similar to the discrete ordinates method inasmuch as discrete directions are chosen. It is also related to the Monte Carlo method (see Chapter 21), since rays of intensity are traced from surface to surface. In essence, nodal points are established on the enclosure's boundary, from which rays are sent out into predetermined directions. The ray is then traced as it traverses through internal finite volumes, and this interaction is recorded (weakening of the ray by depositing energy in the volume, strengthening by emission and in-scattering), until it hits another surface. The method is very similar to the standard DOM and carries its disadvantages (nonconservative, susceptible to ray effects, needs iterations for non-black walls and/or scattering), but uses much more cumbersome beam tracing (equivalent to the exponential scheme). A solid angle "pencil" is established at the emission point, causing inaccuracies as the beam passes through internal volumes. The ray tracing is very similar to that of the Monte Carlo method. While the DTM avoids the statistical scatter of the Monte Carlo method, it is less efficient because each ray carries a single piece of statistic (given location, direction, wavelength), while a statistically chosen bundle in a Monte Carlo simulation carries multiple statistics (particularly important in nongray, reflecting and/or scattering environments). Still, the method enjoys some popularity because of its early arrival, its early ability to deal with irregular geometries, and because it has been incorporated into several important commercial CFD codes. Cumber [151, 152] has offered several improvements for the method, Coelho and Carvalho [153] presented a conservative formulation of the DTM, and Versteeg and coworkers [154, 155] have quantified the errors inherent to the method. Two- and three-dimensional calculations have been performed by several researchers, mostly for furnace and other combustion applications [156–163]. Several comparisons between the DTM and other methods have also been made. Selçuk and Kayakol [68] compared DTM and S_4 solutions for two-dimensional, rectangular geometries and found that the S_4 method gave results of comparable accuracy at three orders of magnitude less computer time. Similarly, Coelho and coworkers [125] solved the radiation problem in two-dimensional enclosures with obstacles, using DTM, DOM, FVM, Monte Carlo, and the zonal method (see Chapter 18); they found DOM and FVM to be the most economical. Finally, Keramida and colleagues employed the DTM and six-flux methods to model natural gas-fired furnaces [150], finding the six-flux method to be superior.

YIX Method. In this method, first developed by Tan and Howell [164], the radiative transfer equation is expressed in integral form [see, for example, equation (10.28)], i.e., incident radiation, G, and radiative flux, q, can be evaluated at any point (inside the medium, or on the boundaries) as a triple integral (in distance away from the point, and in solid angle). Integration away from each point (along discrete ordinates) involves certain geometric functions, which can be predetermined. While this method has the potential to be more efficient than the DOM and the FVM, setup work for each problem is significant and generalization is difficult. The method appears to have been used only by the group that developed it [165–169].

17.10 CONCLUDING REMARKS

The finite volume method, because of its general applicability, and the ability to generate high-accuracy solutions with fine meshes, is today probably the most popular method to solve the RTE in complex situations. To be sure, the method also has its weaknesses: it always requires an iterative solution in the presence of scattering and/or reflecting walls, and for optically thick media these iterations tend to converge very slowly, if at all. In addition, the discrete ordinates method is prone to ray effects and can suffer from false scattering. However, the DOM and FVM are the only methods (aside from the statistical Monte Carlo method) that, through refinement of the spatial and directional grids, can be carried to arbitrary levels of accuracy without adding to its mathematical complexity.

The discrete ordinates method is related to the zonal method of Chapter 18, which was the preferred RTE solution method until the 1960s. The zonal method also performs poorly in optically thick media, but it does not suffer from ray effects and false scattering. However, it cannot be used in the presence of anisotropic scattering, and it is difficult to apply to irregular geometries. The P_1-approximation, on the other hand, is much easier to apply and solve, and gives very accurate results for optically thick media (where DOM and FVM are difficult to apply), as well as for hot, radiating media in cold surroundings. But this method fails in optically thin media surrounded by radiating walls and/or subject to directional irradiation. Importantly, higher orders of the P_N-approximation are mathematically difficult to formulate.

References

1. Chandrasekhar, S.: *Radiative Transfer*, Dover Publications, New York, 1960.
2. Lee, C. E.: "The discrete S_n approximation to transport theory," Technical Information Series Report LA2595, Lawrence Livermore Laboratory, 1962.
3. Lathrop, K. D.: "Use of discrete-ordinate methods for solution of photon transport problems," *Nuclear Science and Engineering*, vol. 24, pp. 381–388, 1966.
4. Carlson, B. G., and K. D. Lathrop: "Transport theory—the method of discrete ordinates," in *Computing Methods in Reactor Physics*, eds. H. Greenspan, C. N. Kelber, and D. Okrent, Gordon & Breach, New York, 1968.
5. Love, T. J., and R. J. Grosh: "Radiative heat transfer in absorbing, emitting, and scattering media," *ASME Journal of Heat Transfer*, vol. 87, pp. 161–166, 1965.
6. Hsia, H. M., and T. J. Love: "Radiative heat transfer between parallel plates separated by a nonisothermal medium with anisotropic scattering," *ASME Journal of Heat Transfer*, vol. 89, pp. 197–204, 1967.
7. Hottel, H. C., A. F. Sarofim, L. B. Evans, and I. A. Vasalos: "Radiative transfer in anisotropically scattering media: Allowance for Fresnel reflection at the boundaries," *ASME Journal of Heat Transfer*, vol. 90, pp. 56–62, 1968.
8. Roux, J. A., D. C. Todd, and A. M. Smith: "Eigenvalues and eigenvectors for solutions to the radiative transport equation," *AIAA Journal*, vol. 10, no. 7, pp. 973–976, 1972.
9. Roux, J. A., and A. M. Smith: "Radiative transport analysis for plane geometry with isotropic scattering and arbitrary temperature," *AIAA Journal*, vol. 12, no. 9, pp. 1273–1277, 1974.
10. Fiveland, W. A.: "A discrete ordinates method for predicting radiative heat transfer in axisymmetric enclosures," ASME Paper 82-HT-20, 1982.
11. Fiveland, W. A.: "Discrete ordinates solutions of the radiative transport equation for rectangular enclosures," *ASME Journal of Heat Transfer*, vol. 106, pp. 699–706, 1984.
12. Fiveland, W. A.: "Discrete ordinate methods for radiative heat transfer in isotropically and anisotropically scattering media," *ASME Journal of Heat Transfer*, vol. 109, pp. 809–812, 1987.
13. Fiveland, W. A.: "Three-dimensional radiative heat-transfer solutions by the discrete-ordinates method," *Journal of Thermophysics and Heat Transfer*, vol. 2, no. 4, pp. 309–316, Oct 1988.
14. Hyde, D. J., and J. S. Truelove: "The discrete ordinates approximation for multidimensional radiant heat transfer in furnaces," Technical Report VKAEA Report No. AERE-R 8502, Thermodynamics Division, AERE Harwell, Oxfordshire, February 1977.
15. Truelove, J. S.: "Discrete-ordinate solutions of the radiation transport equation," *ASME Journal of Heat Transfer*, vol. 109, no. 4, pp. 1048–1051, 1987.
16. Truelove, J. S.: "Three-dimensional radiation in absorbing–emitting–scattering media using the discrete-ordinates approximation," *Journal of Quantitative Spectroscopy and Radiative Transfer*, vol. 39, no. 1, pp. 27–31, 1988.

17. Charest, M. R. J., C. P. T. Groth, and O. L. Gülder: "Solution of the equation of radiative transfer using a Newton-Krylov approach and adaptive mesh refinement," *Journal of Computational Physics*, vol. 231, no. 8, pp. 3023–3040, 2012.
18. Coelho, P. J.: "Discrete ordinates and finite volume methods," *Thermopedia*, 2011, http://www.thermopedia.com.
19. Lathrop, K. D., and B. G. Carlson: "Discrete-ordinates angular quadrature of the neutron transport equation," Technical Information Series Report LASL-3186, Los Alamos Scientific Laboratory, 1965.
20. Carlson, B. G.: "Tables of equal weight quadrature over the unit sphere," Technical Information Series Report LA-4737, Los Alamos Scientific Laboratory, 1971.
21. Fiveland, W. A.: "The selection of discrete ordinate quadrature sets for anisotropic scattering," in *Fundamentals of Radiation Heat Transfer*, vol. HTD-160, ASME, pp. 89–96, 1991.
22. Sánchez, A., and T. F. Smith: "Surface radiation exchange for two-dimensional rectangular enclosures using the discrete-ordinates method," *ASME Journal of Heat Transfer*, vol. 114, pp. 465–472, 1992.
23. El-Wakil, N., and J.-F. Sacadura: "Some improvements of the discrete ordinates method for the solution of the radiative transport equation in multidimensional anisotropically scattering media," in *Developments in Radiative Heat Transfer*, vol. HTD-203, ASME, pp. 119–127, 1992.
24. Thurgood, C. P., A. Pollard, and H. A. Becker: "The T_N quadrature set for the discrete ordinates method," *ASME Journal of Heat Transfer*, vol. 117, no. 4, pp. 1068–1070, 1995.
25. Li, B. W., Q. Yao, X. Y. Cao, and K. F. Cen: "A new discrete ordinates quadrature scheme for three-dimensional radiative heat transfer," *ASME Journal of Heat Transfer*, vol. 120, no. 2, pp. 514–518, 1998.
26. Koch, R., and R. Becker: "Evaluation of quadrature schemes for the discrete ordinates method," *Journal of Quantitative Spectroscopy and Radiative Transfer*, vol. 84, pp. 423–435, 2004.
27. Li, H. S., G. Flamant, and J. D. Lu: "An alternative discrete ordinate scheme for collimated irradiation problems," *International Communications in Heat and Mass Transfer*, vol. 30, no. 1, pp. 61–70, 2003.
28. Kumar, S., A. Majumdar, and C. L. Tien: "The differential-discrete-ordinate method for solutions of the equation of radiative transfer," *ASME Journal of Heat Transfer*, vol. 112, no. 2, pp. 424–429, 1990.
29. *IMSL Math/Library*, 1st ed., IMSL, Houston, TX, 1989.
30. Stamnes, K., and P. Conklin: "A new multi-layer discrete ordinate approach to radiative transfer in vertically inhomogeneous atmospheres," *Journal of Quantitative Spectroscopy and Radiative Transfer*, vol. 31, no. 3, pp. 273–282, 1984.
31. Stamnes, K., S.-C. Tsay, W. J. Wiscombe, and K. Jayaweera: "Numerically stable algorithm for discrete-ordinate-method radiative transfer in multiple scattering and emitting layered media," *Applied Optics*, vol. 27, no. 12, pp. 2502–2509, 1988.
32. Cowell, W. R. (ed.): *Sources and Developments of Mathematical Software*, Prentice Hall, Englewood Cliffs, NJ, 1980.
33. Boulet, P., G. Jeandel, and G. Morlot: "Model of radiative transfer in fibrous media-matrix method," *International Journal of Heat and Mass Transfer*, vol. 36, pp. 4287–4297, 1993.
34. Kim, T. K., J. A. Menart, and H. S. Lee: "Nongray radiative gas analyses using the S-N discrete ordinates method," *ASME Journal of Heat Transfer*, vol. 113, no. 4, pp. 946–952, 1991.
35. Menart, J. A., H. S. Lee, and T. K. Kim: "Discrete ordinates solutions of nongray radiative transfer with diffusely reflecting walls," *ASME Journal of Heat Transfer*, vol. 115, no. 1, pp. 184–193, 1993.
36. Lu, J. D., G. Flamant, and B. Variot: "Theoretical study of combined conductive, convective and radiative heat transfer between plates and packed beds," *International Journal of Heat and Mass Transfer*, vol. 37, no. 5, pp. 727–736, 1994.
37. De Miranda, A. B., and J.-F. Sacadura: "An alternative formulation of the S-N discrete ordinates for predicting radiative transfer in nongray gases," *ASME Journal of Heat Transfer*, vol. 118, no. 3, pp. 650–653, 1996.
38. Hendricks, T. J., and J. R. Howell: "New radiative analysis approach for reticulated porous ceramics using discrete ordinates method," *ASME Journal of Heat Transfer*, vol. 118, no. 4, pp. 911–917, 1996.
39. Jones, P. D., D. G. McLeod, and D. E. Dorai-Raj: "Correlation of measured and computed radiation intensity exiting a packed bed," *ASME Journal of Heat Transfer*, vol. 118, no. 1, pp. 94–102, 1996.
40. Wang, Y., and Y. Bayazitoğlu: "Wavelets and discrete ordinates method in solving one-dimensional nongray radiation problem," *International Journal of Heat and Mass Transfer*, vol. 42, no. 3, pp. 385–393, 1999.
41. Mitra, K., and J. H. Churnside: "Transient radiative transfer equation applied to oceanographic lidar," *Applied Optics*, vol. 38, no. 6, pp. 889–895, 1999.
42. Yao, C., G. X. Wang, and B. T. F. Chung: "Nonequilibrium planar interface model for solidification of semitransparent radiating materials," *Journal of Thermophysics and Heat Transfer*, vol. 14, no. 3, pp. 297–304, 2000.
43. Tsai, J. R., M. N. Özişik, and F. Santarelli: "Radiation in spherical symmetry with anisotropic scattering and variable properties," *Journal of Quantitative Spectroscopy and Radiative Transfer*, vol. 42, no. 3, pp. 187–199, 1989.
44. Jones, P. D., and Y. Bayazitoğlu: "Combined radiation and conduction from a sphere in a participating medium," in *Proceedings of the Ninth International Heat Transfer Conference*, vol. 6, Hemisphere, Washington, D.C., pp. 397–402, 1990.
45. Jones, P. D., and Y. Bayazitoğlu: "Radiation, conduction and convection from a sphere in an absorbing, emitting, gray medium," *ASME Journal of Heat Transfer*, vol. 114, no. 1, pp. 250–254, 1992.
46. Krishnaprakas, C. K.: "Combined conduction and radiation heat transfer in a cylindrical medium," *Journal of Thermophysics and Heat Transfer*, vol. 12, no. 4, pp. 605–608, 1998.
47. Chai, J. C., H. S. Lee, and S. V. Patankar: "Improved treatment of scattering using the discrete ordinates method," *ASME Journal of Heat Transfer*, vol. 116, no. 1, pp. 260–263, 1994.

48. Chai, J. C., S. V. Patankar, and H. S. Lee: "Evaluation of spatial differencing practices for the discrete-ordinates method," *Journal of Thermophysics and Heat Transfer*, vol. 8, no. 1, pp. 140–144, 1994.
49. Lathrop, K. D.: "Spatial differencing of the transport equation: Positivity vs. accuracy," *Nuclear Science and Engineering*, vol. 4, pp. 475–498, 1968.
50. Jamaluddin, A. S., and P. J. Smith: "Predicting radiative transfer in rectangular enclosures using the discrete ordinates method," *Combustion Science and Technology*, vol. 59, pp. 321–340, 1988.
51. Kim, I. K., and W. S. Kim: "A hybrid spatial differencing scheme for discrete ordinates method in 2D rectangular enclosures," *International Journal of Heat and Mass Transfer*, vol. 44, pp. 575–586, 2001.
52. Jessee, J. P., and W. A. Fiveland: "Bounded, high-resolution differencing schemes applied to the discrete ordinates method," *Journal of Thermophysics and Heat Transfer*, vol. 11, no. 4, pp. 540–548, 1997.
53. Leonard, B. P.: "Bounded higher-order upwind multidimensional finite-volume convection–diffusion algorithms," in *Advances in numerical heat transfer*, eds. W. J. Minkowycz and E. M. Sparrow, vol. 1, Taylor & Francis, Washington, DC, pp. 1–57, 1997.
54. Coelho, P. J.: "A comparison of spatial discretization schemes for differential solution methods of the radiative transfer equation," *Journal of Quantitative Spectroscopy and Radiative Transfer*, vol. 109(2), pp. 189–200, 2008.
55. Chai, J. C., H. S. Lee, and S. V. Patankar: "Ray effect and false scattering in the discrete ordinates method," *Numerical Heat Transfer – Part B: Fundamentals*, vol. 24, pp. 373–389, 1993.
56. Coelho, P. J.: "The role of ray effects and false scattering on the accuracy of the standard and modified discrete ordinates methods," *Journal of Quantitative Spectroscopy and Radiative Transfer*, vol. 73(2–5), pp. 231–238, 2002.
57. Li, H. S., G. Flamant, and J. D. Lu: "Mitigation of ray effects in the discrete ordinates method," *Numerical Heat Transfer – Part B: Fundamentals*, vol. 43, no. 5, pp. 445–466, 2003.
58. Chai, J. C., P.-F. Hsu, and Y. C. Lam: "Three-dimensional transient radiative transfer modeling using the finite-volume method," *Journal of Quantitative Spectroscopy and Radiative Transfer*, vol. 86(3), pp. 299–313, 2004.
59. Razzaque, M. M., D. E. Klein, and J. R. Howell: "Finite element solution of radiative heat transfer in a two-dimensional rectangular enclosure with gray participating media," *ASME Journal of Heat Transfer*, vol. 105, pp. 933–936, 1983.
60. Kim, T. K., and H. S. Lee: "Effect of anisotropic scattering on radiative heat transfer in two-dimensional rectangular enclosures," *International Journal of Heat and Mass Transfer*, vol. 31, no. 8, pp. 1711–1721, 1988.
61. Kim, T. K., and H. S. Lee: "Radiative transfer in two-dimensional anisotropic scattering media with collimated incidence," *Journal of Quantitative Spectroscopy and Radiative Transfer*, vol. 42, pp. 225–238, 1989.
62. Baek, S. W., and T. Y. Kim: "The conductive and radiative heat transfer in rectangular enclosure using the discrete ordinates method," in *Proceedings of the Ninth International Heat Transfer Conference*, vol. 6, Hemisphere, Washington, D.C., pp. 433–438, 1990.
63. Kim, T. Y., and S. W. Baek: "Thermal development of radiatively active pipe flow with nonaxisymmetric circumferential convective heat loss," *International Journal of Heat and Mass Transfer*, vol. 39, no. 14, pp. 2969–2976, 1996.
64. Kim, J. S., S. W. Baek, and C. R. Kaplan: "Effect of radiation on diffusion flame behavior over a combustible solid," *Combustion Science and Technology*, vol. 88, no. 1/2, pp. 133–150, 1993.
65. Mesyngier, C., and B. Farouk: "Turbulent natural convection–nongray gas radiation analysis in a square enclosure," *Numerical Heat Transfer – Part A: Applications*, vol. 29, no. 7, pp. 671–687, 1996.
66. Mesyngier, C., and B. Farouk: "Convection–nongray gas radiation interactions in a channel flow," in *Proceedings of the 1996 Heat Transfer Conference*, vol. HTD-325 No. 3, ASME, pp. 103–113, 1996.
67. Wang, H. Y., P. Joulain, and J. M. Most: "Modeling on burning of large-scale vertical parallel surfaces with fire-induced flow," *Fire Safety Journal*, vol. 32, no. 3, pp. 241–247, 1999.
68. Selçuk, N., and N. Kayakol: "Evaluation of discrete ordinates method for radiative transfer in rectangular furnaces," *International Journal of Heat and Mass Transfer*, vol. 40, no. 2, pp. 213–222, 1997.
69. Lockwood, F. C., and N. G. Shah: "A new radiation solution method for incorporation in general combustion prediction procedures," in *Eighteenth Symposium (International) on Combustion*, The Combustion Institute, pp. 1405–1409, 1981.
70. Jamaluddin, A. S., and P. J. Smith: "Predicting radiative transfer in axisymmetric cylindrical enclosures using the discrete ordinates method," *Combustion Science and Technology*, vol. 62, pp. 173–186, 1988.
71. Mengüç, M. P., and R. Viskanta: "Radiative transfer in three-dimensional rectangular enclosures containing inhomogeneous, anisotropically scattering media," *Journal of Quantitative Spectroscopy and Radiative Transfer*, vol. 33, no. 6, pp. 533–549, 1985.
72. Park, H. M., and T. Y. Yoon: "Solution of the inverse radiation problem using a conjugate gradient method," *International Journal of Heat and Mass Transfer*, vol. 43, no. 10, pp. 1767–1776, 2000.
73. Lacroix, D., G. Jeandel, and C. Boudot: "Solution of the radiative transfer equation in an absorbing and scattering Nd:YAG laser-induced plume," *Journal of Applied Physics*, vol. 84, pp. 2443–2449, 1998.
74. Gonçalves, J., and P. J. Coelho: "Parallelization of the discrete ordinates method," *Numerical Heat Transfer – Part B: Fundamentals*, vol. 32, pp. 151–173, 1997.
75. Fiveland, W. A., and J. P. Jessee: "Acceleration schemes for the discrete ordinates method," *Journal of Thermophysics and Heat Transfer*, vol. 10, no. 3, pp. 445–451, 1996.
76. Balsara, D.: "Fast and accurate discrete ordinates methods for multidimensional radiative transfer. Part I: Basic methods," *Journal of Quantitative Spectroscopy and Radiative Transfer*, vol. 69, pp. 671–707, 2001.

77. Jamaluddin, A. S., and P. J. Smith: "Discrete-ordinates solution of radiative transfer equation in non-axisymmetric cylindrical enclosures," in *Proceedings of the 1988 National Heat Transfer Conference*, vol. HTD-96, ASME, pp. 227–232, 1988.
78. Jamaluddin, A. S., and P. J. Smith: "Discrete-ordinates solution of radiative transfer equation in nonaxisymmetric cylindrical enclosures," *Journal of Thermophysics and Heat Transfer*, vol. 6, no. 2, pp. 242–245, 1992.
79. Kim, S. S., and S. W. Baek: "Radiation affected compressible turbulent flow over a backward facing step," *International Journal of Heat and Mass Transfer*, vol. 39, no. 16, pp. 3325–3332, 1996.
80. Kaplan, C. R., S. W. Baek, E. S. Oran, and J. L. Ellzey: "Dynamics of a strongly radiating unsteady ethylene jet diffusion flame," *Combustion and Flame*, vol. 96, pp. 1–21, 1994.
81. Ramamurthy, H., S. Ramadhyani, and R. Viskanta: "A two-dimensional axisymmetric model for combusting, reacting and radiating flows in radiant tubes," *Journal of the Institute of Energy*, vol. 67, pp. 90–100, 1994.
82. Song, M., K. S. Ball, and T. L. Bergman: "A model for radiative cooling of a semitransparent molten glass jet," *ASME Journal of Heat Transfer*, vol. 120, no. 4, pp. 931–938, 1998.
83. Jendoubi, S., H. S. Lee, and T. K. Kim: "Discrete ordinates solutions for radiatively participating media in a cylindrical enclosure," *Journal of Thermophysics and Heat Transfer*, vol. 7, no. 2, pp. 213–219, 1993.
84. Howell, L. H., and V. E. Beckner: "Discrete ordinates algorithm for domains with embedded boundaries," *Journal of Thermophysics and Heat Transfer*, vol. 11, no. 4, pp. 549–555, 1997.
85. Adams, B. R., and P. J. Smith: "Three-dimensional discrete-ordinates modeling of radiative transfer in a geometrically complex furnace," *Combustion Science and Technology*, vol. 88, pp. 293–308, 1993.
86. Sakami, M., A. Charette, and V. Le Dez: "Application of the discrete ordinates method to combined conductive and radiative heat transfer in a two-dimensional complex geometry," *Journal of Quantitative Spectroscopy and Radiative Transfer*, vol. 56, no. 4, pp. 517–533, 1996.
87. Sakami, M., A. Charette, and V. Le Dez: "Radiation heat transfer in three-dimensional enclosures of complex geometry by using the discrete ordinates method," *Journal of Quantitative Spectroscopy and Radiative Transfer*, vol. 59, no. 1-2, pp. 117–136, 1998.
88. Cheong, K. B., and T.-H. Song: "An alternative discrete ordinates method with interpolation and source differencing for two-dimensional radiative transfer problems," *Numerical Heat Transfer – Part B: Fundamentals*, vol. 32, pp. 107–125, 1997.
89. Koo, H. M., K. B. Cheong, and T.-H. Song: "Schemes and applications of first and second-order discrete ordinates interpolation methods to irregular two-dimensional geometries," *ASME Journal of Heat Transfer*, vol. 119, no. 4, pp. 730–737, 1997.
90. Cha, H., and T.-H. Song: "Discrete ordinates interpolation method for solution of radiative transfer equation in arbitrary 2-D geometry and unstructured grid system," in *Proceedings of The 11th International Heat Transfer Conference*, vol. 7, pp. 267–274, 1998.
91. Cha, H., and T.-H. Song: "Discrete ordinates interpolation method applied to irregular three-dimensional geometries," *ASME Journal of Heat Transfer*, vol. 122, no. 4, pp. 823–827, 2000.
92. Seo, S. H., and T. K. Kim: "Study on interpolation schemes of the discrete ordinates interpolation method for three-dimensional radiative transfer with nonorthogonal grids," *ASME Journal of Heat Transfer*, vol. 120, no. 4, pp. 1091–1094, 1998.
93. Patankar, S. V.: *Numerical Heat Transfer and Fluid Flow*, 1st ed., Hemisphere Publishing Corporation, New York, 1980.
94. Fiveland, W. A., and J. P. Jessee: "Finite element formulation of the discrete-ordinates method for multidimensional geometries," *Journal of Thermophysics and Heat Transfer*, vol. 8, no. 3, pp. 426–433, 1994.
95. An, W., L. M. Ruan, H. Qi, and L. H. Liu: "Finite element method for radiative heat transfer in absorbing and anisotropic scattering media," *Journal of Quantitative Spectroscopy and Radiative Transfer*, vol. 96(3-4), pp. 409–422, 2005.
96. Liu, L. H., and J. Y. Tan: "Least-squares collocation meshless approach for radiative heat transfer in absorbing and scattering media," *Journal of Quantitative Spectroscopy and Radiative Transfer*, vol. 103, no. 3, pp. 545–557, 2007.
97. Briggs, L. L., W. F. Miller, Jr., and E. E. Lewis: "Ray-effect mitigation in discrete ordinate-like angular finite element approximations in neutron transport," *Nuclear Science and Engineering*, vol. 57, pp. 205–217, 1975.
98. Raithby, G. D., and E. H. Chui: "A finite-volume method for predicting a radiant heat transfer enclosures with participating media," *ASME Journal of Heat Transfer*, vol. 112, no. 2, pp. 415–423, 1990.
99. Chui, E. H., G. D. Raithby, and P. M. J. Hughes: "Prediction of radiative transfer in cylindrical enclosures with the finite volume method," *Journal of Thermophysics and Heat Transfer*, vol. 6, no. 4, pp. 605–611, 1992.
100. Chui, E. H., and G. D. Raithby: "Computation of radiant heat transfer on a nonorthogonal mesh using the finite-volume method," *Numerical Heat Transfer – Part B: Fundamentals*, vol. 23, pp. 269–288, 1993.
101. Chui, E. H., P. M. J. Hughes, and G. D. Raithby: "Implementation of the finite volume method for calculating radiative transfer in a pulverized fuel flame," *Combustion Science and Technology*, vol. 92, no. 4/6, pp. 225–242, 1993.
102. Chai, J. C., H. S. Lee, and S. V. Patankar: "Finite volume method for radiation heat transfer," *Journal of Thermophysics and Heat Transfer*, vol. 8, no. 3, pp. 419–425, 1994.
103. Chai, J. C., H. S. Lee, and S. V. Patankar: "Treatment of irregular geometries using a Cartesian coordinates finite-volume radiation heat transfer procedure," *Numerical Heat Transfer – Part B: Fundamentals*, vol. 26, pp. 225–235, 1994.

104. Chai, J. C., G. Parthasarathy, H. S. Lee, and S. V. Patankar: "Finite volume method radiative heat transfer procedure for irregular geometries," *Journal of Thermophysics and Heat Transfer*, vol. 9, no. 3, pp. 410–415, 1995.
105. Raithby, G. D.: "Discussion of the finite-volume method for radiation, and its application using 3D unstructured meshes," *Numerical Heat Transfer – Part B: Fundamentals*, vol. 35, no. 4, pp. 389–405, 1999.
106. Wylie, C. R.: *Advanced Engineering Mathematics*, 5th ed., McGraw-Hill, New York, 1982.
107. Chai, J. C.: "One-dimensional transient radiation heat transfer modeling using a finite-volume method," *Numerical Heat Transfer – Part B: Fundamentals*, vol. 44, pp. 1–22, 2003.
108. Modest, M. F., and J. Yang: "Elliptic PDE formulation and boundary conditions of the spherical harmonics method of arbitrary order for general three-dimensional geometries," *Journal of Quantitative Spectroscopy and Radiative Transfer*, vol. 109, pp. 1641–1666, 2008.
109. Murthy, J. Y., and S. R. Mathur: "Finite volume method for radiative heat transfer using unstructured meshes," *Journal of Thermophysics and Heat Transfer*, vol. 12, no. 3, pp. 313–321, 1998.
110. Mathur, S. R., and J. Y. Murthy: "Radiative heat transfer in periodic geometries using a finite volume scheme," *ASME Journal of Heat Transfer*, vol. 121, no. 2, pp. 357–364, 1999.
111. Mathur, S. R., and J. Y. Murthy: "Coupled ordinates method for multigrid acceleration of radiation calculations," *Journal of Thermophysics and Heat Transfer*, vol. 13, no. 4, pp. 467–473, 1999.
112. Mathur, S. R., and J. Y. Murthy: "Acceleration of anisotropic scattering computations using coupled ordinates method (Comet)," *ASME Journal of Heat Transfer*, vol. 123, no. 3, pp. 607–612, 1999.
113. Hassanzadeh, P., G. D. Raithby, and E. H. Chui: "Efficient calculation of radiation heat transfer in participating media," *Journal of Thermophysics and Heat Transfer*, vol. 22, no. 2, pp. 129–139, 2008.
114. Kim, S. H., and K. Y. Huh: "A new angular discretization scheme of the finite volume method for 3-D radiative heat transfer in absorbing, emitting and anisotropically scattering media," *International Journal of Heat and Mass Transfer*, vol. 43, no. 7, pp. 1233–1242, 2000.
115. Liu, J., H. M. Shang, and Y. S. Chen: "Parallel simulation of radiative heat transfer using an unstructured finite-volume method," *Numerical Heat Transfer – Part B: Fundamentals*, vol. 36, no. 2, pp. 115–137, 1999.
116. Martin, A. R., C. Saltiel, J. C. Chai, and W. Shyy: "Convective and radiative internal heat transfer augmentation with fiber arrays," *International Journal of Heat and Mass Transfer*, vol. 41, pp. 3431–3440, 1998.
117. Bergero, S., E. Nannei, and R. Sala: "Combined radiative and convective heat transfer in a three-dimensional rectangular channel at different wall temperatures," *Wärme- und Stoffübertragung*, vol. 36, no. 6, pp. 443–450, 1999.
118. *ANSYS FLUENT Computational Fluid Dynamics Software*, ANSYS Corp., Canonsburg, Pennsylvania, 2011.
119. Cui, X., and B. Q. Li: "Discontinuous finite element solution of 2-D radiative transfer with and without axisymmetry," *Journal of Quantitative Spectroscopy and Radiative Transfer*, vol. 96(3-4), pp. 383–407, 2005.
120. Grissa, H., F. Askri, M. B. Salah, and S. Ben Nasrallah: "Three-dimensional radiative transfer modeling using the control volume finite element method," *Journal of Quantitative Spectroscopy and Radiative Transfer*, vol. 105, no. 3, pp. 388–404, 2007.
121. Liu, J., H. M. Shang, Y. S. Chen, and T. S. Wang: "Analysis of discrete ordinates method with even parity formulation," *Journal of Thermophysics and Heat Transfer*, vol. 11, no. 2, pp. 253–260, 1997.
122. Thompson, J. F., Z. U. A. Warsi, and C. W. Mastin: *Numerical Grid Generation, Foundations and Applications*, North-Holland, New York, 1985.
123. Fiveland, W. A., and J. P. Jessee: "Comparison of discrete ordinates formulations for radiative heat transfer in multidimensional geometries," *Journal of Thermophysics and Heat Transfer*, vol. 9, no. 1, pp. 47–54, 1995.
124. Kim, S. H., and K. Y. Huh: "Assessment of the finite-volume method and the discrete ordinate method for radiative heat transfer in a three-dimensional rectangular enclosure," *Numerical Heat Transfer – Part B: Fundamentals*, vol. 35, no. 1, pp. 85–112, 1999.
125. Coelho, P. J., J. Gonçalves, and M. G. Carvalho: "Modelling of radiative heat transfer in enclosures with obstacles," *International Journal of Heat and Mass Transfer*, vol. 41, no. 4, pp. 745–756, 1998.
126. Baek, S. W., and M. Y. Kim: "Analysis of radiative heating of a rocket plume base with the finite-volume method," *International Journal of Heat and Mass Transfer*, vol. 40, no. 7, pp. 1501–1508, 1997.
127. Baek, S. W., M. Y. Kim, and J. S. Kim: "Nonorthogonal finite-volume solutions of radiative heat transfer in a three-dimensional enclosure," *Numerical Heat Transfer – Part B: Fundamentals*, vol. 34, pp. 419–437, 1998.
128. Baek, S. W., D. Y. Byun, and S. J. Kang: "The combined Monte-Carlo and finite-volume method for radiation in a two-dimensional irregular geometry," *International Journal of Heat and Mass Transfer*, vol. 43, no. 13, pp. 2337–2344, 2000.
129. Ramankutty, M. A., and A. L. Crosbie: "Modified discrete ordinates solution of radiative transfer in two-dimensional rectangular enclosures," *Journal of Quantitative Spectroscopy and Radiative Transfer*, vol. 57, pp. 107–140, 1997.
130. Ramankutty, M. A., and A. L. Crosbie: "Modified discrete ordinates solution of radiative transfer in three-dimensional rectangular enclosures," *Journal of Quantitative Spectroscopy and Radiative Transfer*, vol. 60, no. 1, pp. 103–134, 1998.
131. Sakami, M., and A. Charette: "Application of a modified discrete ordinates method to two-dimensional enclosures of irregular geometry," *Journal of Quantitative Spectroscopy and Radiative Transfer*, vol. 64, pp. 275–298, 2000.

132. Sakami, M., A. El Kasmi, and A. Charette: "Analysis of radiative heat transfer in complex two-dimensional enclosures with obstacles using the modified discrete ordinates method," *International Journal of Heat and Mass Transfer*, vol. 123, pp. 892–900, 2001.
133. Byun, D. Y., C. Lee, and S. W. Baek: "Radiative heat transfer in discretely heated irregular geometry with an absorbing, emitting, and anisotropically scattering medium using combined Monte-Carlo and finite volume method," *International Journal of Heat and Mass Transfer*, vol. 47, pp. 4195–4203, 2004.
134. Li, H. S., and J. Werther: "Computation of radiative image formation in isolated source and collimated irradiation problems," *Journal of Quantitative Spectroscopy and Radiative Transfer*, vol. 97, pp. 142–159, 2006.
135. Song, T.-H., and C. W. Park: "Formulation and application of the second-order discrete ordinate method," in *Transport Phenomena and Science*, ed. B.-X. Wang, Higher Education Press, Beijing, pp. 833–841, 1992.
136. Koch, R., W. Krebs, S. Wittig, and R. Viskanta: "A parabolic formulation of the discrete ordinates method for the treatment of complex geometries," in *Proceedings of the First International Symposium on Radiation Transfer*, ed. M. P. Mengüç, Begell House, pp. 193–208, 1996.
137. Liu, J., H. M. Shang, Y. S. Chen, and T. S. Wang: "Analysis of discrete ordinates method with even parity formulation," *Journal of Thermophysics and Heat Transfer*, vol. 11, no. 2, pp. 253–260, 1997.
138. Kang, S. H., and T. H. Song: "Finite element formulation of the first- and second-order discrete ordinates equations for radiative heat transfer calculation in three-dimensional participating media," *Journal of Quantitative Spectroscopy and Radiative Transfer*, vol. 109, no. 11, pp. 2094–2107, 2008.
139. Becker, R., R. Koch, H.-J. Bauer, and M. F. Modest: "A finite element treatment of the angular dependency of the even-parity equation of radiative transfer," *ASME Journal of Heat Transfer*, vol. 132, p. 023404, 2010.
140. Jeandel, G., P. Boulet, and G. Morlot: "Radiative transfer through a medium of silica fibers oriented in parallel planes," *International Journal of Heat and Mass Transfer*, vol. 36, no. 2, pp. 531–536, 1993.
141. Argento, C., and D. Bouvard: "A ray tracing method for evaluating the radiative heat transfer in porous media," *International Journal of Heat and Mass Transfer*, vol. 39, pp. 3175–3180, 1996.
142. Siegel, R., and C. M. Spuckler: "Approximate solution methods for spectral radiative transfer in high refractive index layers," *International Journal of Heat and Mass Transfer*, vol. 37, pp. 403–413, 1994.
143. Spuckler, C. M., and R. Siegel: "Two-flux and diffusion methods for radiative transfer in composite layers," *ASME Journal of Heat Transfer*, vol. 118, pp. 218–222, 1996.
144. Tremante, A., and F. Malpica: "Analysis of the temperature profile of ceramic composite materials exposed to combined conduction–radiation between concentric cylinders," *Journal of Engineering for Gas Turbines and Power*, vol. 120, no. 2, pp. 271–275, 1998.
145. Dembele, S., J. X. Wen, and J.-F. Sacadura: "Analysis of the two-flux model for predicting water spray transmittance in fire protection application," *ASME Journal of Heat Transfer*, vol. 122, no. 1, pp. 183–186, 2000.
146. Chu, C. M., and S. W. Churchill: "Numerical solution of problems in multiple scattering of electromagnetic radiation," *Journal of Physical Chemistry*, vol. 59, pp. 855–863, 1960.
147. Chin, J. H., and S. W. Churchill: "Anisotropic, multiply scattered radiation from an arbitrary, cylindrical source in an infinite slab," *ASME Journal of Heat Transfer*, vol. 87, pp. 167–172, 1965.
148. Daniel, K. J., N. M. Laurendeau, and F. P. Incropera: "Prediction of radiation absorption and scattering in turbid water bodies," *ASME Journal of Heat Transfer*, vol. 101, pp. 63–67, 1979.
149. Sasse, C., R. Königsdorff, and S. Frank: "Evaluation of an improved hybrid six-flux/zone model for radiative transfer in rectangular enclosures," *International Journal of Heat and Mass Transfer*, vol. 38, pp. 3423–3431, 1995.
150. Keramida, E. P., H. H. Liakos, and M. A. Founti: "Radiative heat transfer in natural gas-fired furnaces," *International Journal of Heat and Mass Transfer*, vol. 43, no. 10, pp. 1801–1809, 2000.
151. Cumber, P. S.: "Improvements to the discrete transfer method of calculating radiative heat transfer," *International Journal of Heat and Mass Transfer*, vol. 38, pp. 2251–2258, 1995.
152. Cumber, P. S.: "Application for adaptive quadrature to fire radiation modeling," *ASME Journal of Heat Transfer*, vol. 121, no. 1, pp. 203–205, 1999.
153. Coelho, P. J., and M. G. Carvalho: "A conservative formulation of the discrete transfer method," *ASME Journal of Heat Transfer*, vol. 119, pp. 118–128, 1997.
154. Versteeg, H. K., J. C. Henson, and W. M. G. Malalasekera: "Approximation errors in the heat flux integral of the discrete transfer method, part 1: Transparent media," *Numerical Heat Transfer – Part B: Fundamentals*, vol. 36, no. 4, pp. 387–407, 1999.
155. Versteeg, H. K., J. C. Henson, and W. M. G. Malalasekera: "Approximation errors in the heat flux integral of the discrete transfer method, part 2: Participating media," *Numerical Heat Transfer – Part B: Fundamentals*, vol. 36, no. 4, pp. 409–432, 1999.
156. Carvalho, M. G., T. L. Farias, and P. Fontes: "Multidimensional modeling of radiative heat transfer in scattering media," *ASME Journal of Heat Transfer*, vol. 116, no. 2, pp. 486–488, May 1993.
157. Malalasekera, W. M. G., and E. H. James: "Radiative heat transfer calculations in three-dimensional complex geometries," *ASME Journal of Heat Transfer*, vol. 118, pp. 225–228, 1996.
158. Henson, J. C., and W. M. G. Malalasekera: "Comparison of the discrete transfer and Monte Carlo methods for radiative heat transfer in three-dimensional nonhomogeneous scattering media," *Numerical Heat Transfer – Part A: Applications*, vol. 32, no. 1, pp. 19–36, 1997.
159. Bressloff, N. W., J. B. Moss, and P. A. Rubini: "CFD prediction of coupled radiation heat transfer and soot production in turbulent flames," in *Proceedings of Twenty-Sixth Symposium (International) on Combustion*, vol. 2, The Combustion Institute, pp. 2379–2386, 1996.

160. Visona, S. P., and B. R. Stanmore: "3-D modelling of NOx formation in a 275 MW utility boiler," *Journal of the Institute of Energy*, vol. 69, pp. 68–79, 1996.
161. Beeri, Z., C. A. Blunsdon, and W. M. G. Malalasekera: "Comprehensive modeling of turbulent flames with the coherent flame-sheet model — part II: High-momentum reactive jets," *Journal of Energy Resources Technology*, vol. 118, pp. 72–76, 1996.
162. Yuan, J., V. Semião, and M. G. Carvalho: "Predictions of particulate formation, oxidation and distribution in a three-dimensional oil-fired furnace," *Journal of the Institute of Energy*, vol. 70, pp. 57–70, 1997.
163. Novo, P. J., P. J. Coelho, and M. G. Carvalho: "Parallelization of the discrete transfer method," *Numerical Heat Transfer – Part B: Fundamentals*, vol. 35, no. 2, pp. 137–161, 1999.
164. Tan, Z. M., and J. R. Howell: "A new numerical method for radiation heat transfer in nonhomogeneous participating media," *Journal of Thermophysics and Heat Transfer*, vol. 4, no. 4, pp. 419–424, 1990.
165. Hsu, P.-F., Z. M. Tan, and J. R. Howell: "Radiative transfer by the YIX method in nonhomogeneous, scattering, and nongray media," *Journal of Thermophysics and Heat Transfer*, vol. 7, no. 3, pp. 487–495, 1993.
166. Hsu, P.-F., and J. C. Ku: "Radiative heat transfer in finite cylindrical enclosures with nonhomogeneous participating media," *Journal of Thermophysics and Heat Transfer*, vol. 8, no. 3, pp. 434–440, 1994.
167. Hsu, P.-F., and J. T. Farmer: "Benchmark solutions of radiative heat transfer within nonhomogeneous participating media using the Monte Carlo and YIX method," *ASME Journal of Heat Transfer*, vol. 119, pp. 185–188, 1997.
168. Hsu, P.-F., and Z. M. Tan: "Radiative and combined-mode heat transfer within L-shaped nonhomogeneous and nongray participating media," *Numerical Heat Transfer – Part A: Applications*, vol. 31, no. 8, pp. 819–835, 1997.
169. Tan, Z. M., P.-F. Hsu, S. H. Wu, and C. Y. Wu: "Modified YIX method and pseudoadaptive angular quadrature for ray effects mitigation," *Journal of Thermophysics and Heat Transfer*, vol. 14, no. 3, pp. 289–296, 2000.

Problems

17.1 Consider a gray, isothermal and isotropically scattering medium contained between large, isothermal, gray plates at temperatures T_1 and T_2, and emittances ϵ_1 and ϵ_2, respectively. Determine the radiative flux between the plates using the S_2-approximation.

17.2 Consider a large, isothermal (temperature T_w), gray and diffuse (emittance ϵ) wall adjacent to a semi-infinite gray absorbing/emitting and linear-anisotropically scattering medium. The medium is isothermal (temperature T_m). Determine the radiative flux as a function of distance away from the plate using the S_2-approximation.

17.3 Consider parallel, black plates, spaced 1 m apart, at constant temperatures T_1 and T_2. Due to pressure variations, the (gray) absorption coefficient is equal to

$$\kappa = \kappa_1 + \kappa_1 x; \quad \kappa_0 = 0.01\,\mathrm{cm}^{-1}; \quad \kappa_1 = 0.0002\,\mathrm{cm}^{-2},$$

where x is measured from plate 1. The medium does not scatter radiation. Determine, for radiative equilibrium, the nondimensional heat flux $\Psi = q/\sigma(T_1^4 - T_2^4)$ by the exact method, and the S_2-approximation.

17.4 Black spherical particles of 100 μm radius are suspended between two cold and black parallel plates 1 m apart. The particles produce heat at a rate of $\pi/10$ W/particle, which must be removed by thermal radiation. The number of particles between the plates is given by

$$N_T(z) = N_0 + \Delta N z/L, \quad 0 < z < L; \qquad N_0 = \Delta N = 212\ \text{particles/cm}^3.$$

(*a*) Determine the local absorption coefficient and the local heat production rate; introduce an optical coordinate and determine the optical thickness of the entire gap.
(*b*) If the S_2-approximation is to be employed, what are the relevant equations and boundary conditions governing the heat transfer?
(*c*) What are the heat flux rates at the top and bottom surfaces? What is the entire amount of energy released by the particles? What is the maximum particle temperature?

17.5 Two infinitely long, concentric cylinders of radii R_1 and R_2 with emittances ϵ_1 and ϵ_2 have the same constant surface temperature T_w. The medium between the cylinders has a constant absorption coefficient κ and does not scatter; uniform heat generation $\dot{Q}'''$ takes place inside the medium. Determine the temperature distribution in the medium and heat fluxes at the wall if radiation is the only means of heat transfer, using the S_2-approximation.

17.6 An infinite, black, isothermal plate bounds a semi-infinite space filled with black spheres. At any given distance z away from the plate the particle number density is identical, namely, $N_T = 6.3662 \times 10^8\ \mathrm{m}^{-3}$. However, the radius of the suspended spheres diminishes monotonically away from the surface as

$$a = a_o\, e^{-z/L}; \qquad a_o = 10^{-4}\,\mathrm{m}, \qquad L = 1\,\mathrm{m}.$$

(*a*) Determine the absorption coefficient as a function of z (you may make the large-particle assumption).

(*b*) Determine the optical coordinate as a function of z. What is the total optical thickness of the semi-infinite space?

(*c*) Assuming that radiative equilibrium prevails and using the S_2-approximation, set up the boundary conditions and solve for heat flux and temperature distribution (as a function of z).

17.7 Consider two parallel black plates, both at 1000 K, that are 2 m apart. The medium between the plates emits and absorbs (but does not scatter) with an absorption coefficient of $\kappa = 0.05236\,\mathrm{cm}^{-1}$ (gray medium). Heat is generated by the medium according to the formula

$$\dot{Q}''' = C\sigma T^4, \qquad C = 6.958 \times 10^{-4}\mathrm{cm}^{-1},$$

where T is the local temperature of the medium between the plates. Assuming that radiation is the only important mode of heat transfer, determine the heat flux to the plates using the (symmetric) S_2-approximation.

17.8 A furnace burning pulverized coal may be approximated by a gray cylinder at radiative equilibrium with uniform heat generation $\dot{Q}''' = 0.266\,\mathrm{W/cm}^3$, bounded by a cold black wall. The gray and constant absorption and scattering coefficients are, respectively, $0.16\,\mathrm{cm}^{-1}$ and $0.04\,\mathrm{cm}^{-1}$, while the furnace radius is $R = 0.5$ m. Scattering may be assumed to be isotropic. Using the S_2-approximation:

(*a*) Set up the relevant equations and their boundary conditions.

(*b*) Calculate the total heat loss from the furnace (per unit length).

(*c*) Calculate the radial temperature distribution; what are the centerline and the adjacent-to-wall temperatures?

(*d*) Qualitatively, if the extinction coefficient is kept constant, what is the effect of varying the scattering coefficient on (*i*) heat transfer rates, (*ii*) temperature levels?

17.9 Estimate the radial temperature distribution in the sun. You may make the following assumptions:

(*i*) The sun is a sphere of radius R.

(*ii*) As a result of high temperatures in the sun, the absorption and scattering coefficients may be approximated to be constant, i.e., $\kappa_\nu, \beta_\nu = \mathrm{const} \neq f(\nu, T, r)$ (free–free transitions!).

(*iii*) As a result of high temperatures, radiation is the only mode of heat transfer.

(*iv*) The fusion process may be approximated by assuming that a small sphere at the center of the sun releases heat uniformly corresponding to the total heat loss of the sun (i.e., assume the sun to be concentric spheres with a certain flux at the inner boundary $r = r_i$).

(*a*) Relate the heat production to the effective sun temperature $T_{\mathrm{eff}} = 5777$ K.

(*b*) Would you expect the sun to be optically thin, intermediate, or thick? Why? What are the prevailing boundary conditions?

(*c*) Find an expression for the temperature distribution (for $r > r_i$) using the S_2-approximation.

(*d*) What is the surface temperature of the sun?

17.10 Repeat Problem 17.9 but replace assumption (*iv*) by the following: The fusion process may be approximated by assuming that the sun releases heat uniformly throughout its volume corresponding to the total heat loss of the sun.

17.11 Consider a sphere of very hot dissociated gas of radius 5 cm. The gas may be approximated as a gray, linear-anisotropically scattering medium with $\kappa = 0.1\,\text{cm}^{-1}$, $\sigma_s = 0.2\,\text{cm}^{-1}$, $A_1 = 1$. The gas is suspended magnetically in vacuum within a large cold container and is initially at a uniform temperature $T_g = 10{,}000\,\text{K}$. Using the S_2-approximation and neglecting conduction and convection, specify the total heat loss per unit time from the entire sphere at time $t = 0$. Outline the solution procedure for times $t > 0$.
Hint: Solve the governing equation by introducing a new dependent variable $g(\tau) = \tau(4\pi I_b - G)$.

17.12 Consider a gray, isothermal, isotropically-scattering medium contained between large, cold, black plates. Determine the local radiative heat flux using the S_4-method. To this purpose, set up the analytical solution using the method of successive approximations, i.e., guess a radiative source function, $S(\tau)$, which is to be improved by successive iterations. Carry out one successive approximation.

17.13 Reconsider Problem 17.12 for a similar medium at radiative equilibrium contained between isothermal black plates at temperatures T_1 and T_2, respectively.

17.14 A hot gray medium is contained between two concentric black spheres of radius $R_1 = 10\,\text{cm}$ and $R_2 = 20\,\text{cm}$. The surfaces of the spheres are isothermal at $T_1 = 2000\,\text{K}$ and $T_2 = 500\,\text{K}$, respectively. The medium absorbs, emits with $n = 1, \kappa = 0.05\,\text{cm}^{-1}$, but does not scatter radiation. Determine the heat flux between the spheres using the S_4-approximation. Compare your results with those of Table 14.2.
Note: This problem requires the numerical solution of four simultaneous simple ordinary differential equations.

17.15 Repeat Problem 17.2 using the finite volume method. Use the upper and lower hemispheres as solid angle ranges.

17.16 Repeat Problem 17.10 using the finite volume method. Use the upper and lower hemispheres as solid angle ranges.

17.17 Repeat Problem 17.12 with the finite volume method, using a total of four solid angle ranges.

(a) Use the solid angle ranges of Example 17.6.

(b) Alternatively, let the z-axis point from plate to plate (with polar angle θ measured from it) and choose:

$$\begin{aligned}
\Omega_1: &\quad 0 \le \psi < \frac{\pi}{2}, &\quad 0 \le \theta \le \pi,\\
\Omega_2: &\quad \frac{\pi}{2} \le \psi < \pi, &\quad 0 \le \theta \le \pi,\\
\Omega_3: &\quad \pi \le \psi < \frac{3\pi}{2}, &\quad 0 \le \theta \le \pi,\\
\Omega_4: &\quad \frac{3\pi}{2} \le \psi < 2\pi, &\quad 0 \le \theta \le \pi.
\end{aligned}$$